Large-scale topography of the North Tibetan ranges as a proxy to contrasted crustal-scale deformation modes

Marc Jolivet, Feng Cheng, Andrew V Zuza, Zhaojie Guo, Olivier Dauteuil

Accepted Manuscript

Journal of the Geological Society

Large-scale topography of the North Tibetan ranges as a proxy to contrasted crustal-scale deformation modes

Marc Jolivet, Feng Cheng, Andrew V. Zuza, Zhaojie Guo & Olivier Dauteuil

DOI: https://doi.org/10.1144/jgs2021-085

To access the most recent version of this article, please click the DOI URL in the line above. When citing this article please include the above DOI.

This article is part of the Fold-and-thrust belts collection available at: https://www.lyellcollection.org/cc/fold-and-thrust-belts

Received 5 July 2021
Revised 26 January 2022
Accepted 10 February 2022

Supplementary material at https://doi.org/10.6084/m9.figshare.c.5841461

Large-scale topography of the North Tibetan ranges as a proxy to contrasted crustal-scale deformation modes

MARC JOLIVET[1,*], FENG CHENG[2], ANDREW V. ZUZA[3], ZHAOJIE GUO[2], OLIVIER DAUTEUIL[1]

[1] Géosciences Rennes–UMR CNRS 6118, Univ Rennes, Rennes, France

[2] Key Laboratory of Orogenic Belts and Crustal Evolution, School of Earth and Space Sciences, Ministry of Education, Peking University, Beijing, China

[3]Nevada Bureau of Mines and Geology, University of Nevada, Reno, NV, USA

* Correspondance marc.jolivet@univ-rennes1.fr

Abbreviated title: Crustal deformation modes of North Tibet

Abstract

Forming the northern margin of the Cenozoic Himalayan – Tibetan orogen, the area surrounding the Qaidam Basin is a key region to study the mechanisms that govern the long-term evolution of intra-continental orogenic processes. Indeed tectonic deformation in that region involves newly-formed and inherited crustal and lithospheric structures, partition between horizontal and vertical movements, as well as a strong influence from external factors such as climate and erosion. This work proposes a description of the topography and crustal structure of the north Tibet ranges as an insight on their tectonic deformation characteristics. The topographic study includes the integrated analysis of regional topographic profiles, river profiles, slope maps and thermochronology data. The available geophysical, geological and structural data are used to draw regional, crustal-scale

geological sections across Northern Tibet to describe the regional crustal structure. We show that three deformation modes are expressed – block uplift, distributed shortening and crustal buckling – in structural compartments that involve either complete mountain ranges or some specific regions inside those ranges. We propose that a new crustal structure may develop parallel to the Altyn Tagh fault, connecting the eastern tip of the Qimen Tagh with the Haiyuan fault, across the Qaidam Basin.

Keywords: Tibet, Cenozoic deformation, Geomorphology, Geological cross-sections, Crustal structure.

Authors contributions: MJ: conceptualization (lead), data curation (lead), writing – original draft (lead), writing – review and editing (lead); FC, AVZ, ZG and OD: conceptualization (supporting), writing – original draft (supporting), writing – review and editing (supporting).

Data availability statements: All data generated or analysed during this study are included in this published article (and its supplementary figures) or in cited references.

Introduction

The topographic and tectonic evolution of the ranges that surround the Qaidam Basin in northern Tibet are central to understand the intracontinental evolution of the major Cenozoic Himalayan – Tibetan collisional orogen. These ranges have been, and are still, the object of a number of important studies (e.g. Tapponnier et al., 1990; Matte et al., 1996; Meyer et al., 1998; Mock et al., 1999; Jolivet et al., 2001; Yin et al., 2007a, 2008; Cheng et al., 2015a, b; Allen et al., 2017; Groves et al., 2020; Wu et al., 2020; Wang et al., 2021) (Fig. 1). For example, deciphering the modalities of the northward propagation of the Tibetan plateau requires understanding the interaction and partitioning between large strike-slip and thrust faults in a single regional stress-field. Northern Tibet includes some of the largest strike-slip faults in Asia such as the left-slip Kunlun, Altyn Tagh and Haiyuan faults, directly associated to major fold and thrust belts such as the Qilian Shan (Molnar and Tapponnier, 1975; Peltzer et al., 1989; Lasserre et al., 1999; Jolivet et al., 2001). Again, the topographic evolution of the plateau and of orogenic domains in general is closely controlled by the complex interactions between tectonic, erosion, sedimentation andclimate. The long-since endorheic Qaidam Basin offers a unique sedimentary archive to address these processes (e.g., Heermance et al., 2013; Chang et al., 2015; Cheng et al., 2015b, 2021a; Ji et al., 2017).

All these topics are strongly dependent on a precise understanding of the regional structural pattern and deformation style. Structural, geomorphology and geochronology studies have thus focused on establishing a precise timing of the deformation (e.g., Mock et al., 1999; George et al., 2001; Jolivet et al., 2001; Clark et al., 2010; Lease et al., 2011; Duvall et al., 2013; Yuan et al., 2013; Li et al., 2019, 2020; Staisch et al., 2020) and determining deformation rates and magnitudes along major structures (e.g. Meyer et al., 1998; Yue et al., 2003; Yin et al., 2007a, 2008; Cheng et al., 2015a; Fu and Awata, 2007; Zuza et al., 2016, 2018; Wu et al., 2020; Liu et al., 2021). The kinematic evolution of northern Tibet in response to the Cenozoic India-Asia collision has been summarized in two end-member models: 1) a progressive, in-sequence migration of the deformation initiating in

the East Kunlun Shan during the late Eocene – Oligocene and reaching the eastern front of the Qilian Shan during middle to late Miocene (England and Houseman, 1985; Meyer et al., 1998; Tapponnier et al., 2001; Zheng et al., 2017) or 2) an initial, Eocene re-activation of inherited strike-slip structures such as the Altyn Tagh fault, rapidly transmitting the deformation to the northern Qilian Shan, followed by out-of-sequence thrusting in the East Kunlun during the Oligocene and progressive northward propagation and increase of that compression throughout the Miocene (Jolivet et al., 2001; Yin et al., 2008; Duvall et al., 2011; Zuza et al., 2019). Many of the major faults in North Tibet such as the Altyn Tagh, Kunlun or Haiyuan faults, are largely inherited from pre-Cenozoic orogenesis and were re-activated in response to the India-Asia collision (Jolivet et al., 1999; 2001; Yin and Harrison, 2000; Sobel et al., 2001; Cheng et al., 2016; Zuza et al., 2018). However, large differences exist in the topography of those various ranges or even inside a single range. These differences have been poorly addressed although they may reflect major mechanisms in crustal and/or lithospheric deformation processes. For example, in the East Kunlun Shan, the topography of the western part of the range (the Qimen Tagh) is shaped by several narrow, largely spaced sub-ranges while further to the east, the range is unique, mainly controlled by a frontal thrust and the Kunlun strike-slip fault (Fig. 1) (Cheng et al., 2014).

In this work, we first compiled available geological, structural and geophysical data to build regional, crustal-scale geological cross-sections. We then use large-scale geomorphic analysis, including cross-ranges topographic profiles, river-bed longitudinal profiles and slope maps to characterize the various topographic compartments in northern Tibet. Comparing the topography with the structural information and long-term exhumation rates derived from low temperature thermochronology data we discuss the topographic compartments in terms of deformation mode. Our analysis suggests that three different deformation modes namely: block uplift, distributed shortening and crustal buckling, are active in northern Tibet. We finally propose that a new crustal structure may develop parallel to the Altyn Tagh fault, running from the eastern tip of the Qimen Tagh, across the Qaidam Basin and the Qilian Shan to finally merge with the Haiyuan fault. This

result suggests that while most of the present-day major strike-slip faults in northern Tibet are inherited, new crustal-scale structures may be initiating to accommodate the continuously increasing compressive strain.

Geological setting and regional geological cross-sections

A number of large-scale cross sections have been drawn across northern Tibet (Meyer et al., 1998), the Qaidam Basin (Yin et al., 2007a, 2008; Cheng et al., 2016, 2017) or the various ranges of northern Tibet (Wittlinger et al., 1998; Jolivet et al., 2003; Craddock et al., 2014; Li et al., 2021; Wang et al., 2021). However, only few addressed the integrated regional crustal-scale structure and the relation between the various basins and ranges (Meyer et al., 1998; Yin et al., 2007a, 2008; Craddock et al., 2014). In order to propose a crustal-scale Cenozoic deformation model for northern Tibet we thus compiled the geological, structural and geophysical data available for the various ranges and compiled them into three representative regional cross-sections (Fig. 2).

Altun Shan range

The Altun Shan range forms the northern limit of the Tibetan plateau, separating the Tarim Basin from the Qaidam Basin (Figs. 1, 2a and 3). Except in the intra-mountain Xorkol Basin that forms the central part of the range, the exposed lithologies mainly consist in Archean, Proterozoic and Paleozoic igneous and metamorphic rocks (Jolivet et al., 1999; Chen et al., 2003; Cowgill et al., 2003; Gehrels et al., 2003; Mattinson et al., 2007; Wang et al., 2013; Zhang et al., 2014). These include Early Paleozoic ophiolitic series (corresponding to a middle Silurian – middle Devonian suture zone (Sobel and Arnaud, 1999)) exposed along the Altyn Tagh fault that limits the range to the south. The nature of the 150 km-long triangular-shaped Xorkol Basin (Fig. 1a) is still debated: it has been interpreted as a pull-apart basin (Guo et al., 1998), a fragment of the Qaidam Basin (Chen et al., 2004) or a Cenozoic transtensive basin accommodating oroclinal bending along the Altyn

Tagh fault system (Wang et al., 2008). The basin is filled with Paleogene to Quaternary clastic deposits, sometimes unconformably on Jurassic series (Ritts et al., 2004; Wang et al., 2006, 2008; Li et al., 2018). North and west of the Xorkol Basin, large patches of Quaternary deposits cover the basement.

The deformation and topographic growth of the Altun Shan is driven both by the sinistral strike-slip motion along the major Altyn Tagh fault and by lithospheric subduction (Fig. 2a). However, the subduction polarity is debated, two opposing models proposing either southward subduction of the Tarim lithosphere beneath the Qaidam and Kunlun blocks (Wittlinger et al., 1998; Jiang et al., 2004; Zhao et al., 2006; Zhang et al., 2015) or northward subduction of the Kunlun lithosphere below the Tarim block lithosphere (Cowgill et al., 2003). The proposed onset time of movement along the Altyn Tagh fault is still highly debated from Eocene to Miocene and the suggested amount of offset varies between 90 and 1200 km with a major consensus between 300 and 400 km (Tapponnier et al., 1986; Ritts and Biffi, 2000; Yin and Harrison, 2000; Jolivet et al., 2001; Gehrels et al., 2003; Darby et al., 2005; Yin et al., 2008; Searle et al., 2011; Cheng et al., 2015a, 2016). This motion accommodated the northeastward displacement of the Qaidam block and the correlative shortening in the Qilian Shan (Jolivet et al., 2001; Yin et al., 2002, 2008; Cheng et al., 2015a, 2016; 2021b).

East Kunlun Shan range

Separating the Qaidam Basin from the Bayan Har terrane to the south (Fig. 1), the East Kunlun Shan is composed of Proterozoic to Paleozoic igneous and metamorphic basement overlain by Triassic and Jurassic sediments (Ministry of Geology and natural resources, 1980; Harris et al., 1988; Mock et al., 1999) (Figs. 4 and 2b,c). The basement also contains ophiolitic mélanges and suture zone materials, including the Permian – Triassic Kunlun-Anyemaqen suture that corresponds to the closure of the Palaeo-Tethys ocean (Konstantinovskaya et al., 2003; Wu et al., 2016, 2019). Similarly to the Altun Shan, the deformation and topographic growth of the East Kunlun Shan is

controlled both by the sinistral strike-slip motion along the Kunlun fault, and the southward subduction of the Qaidam lithosphere under the Kunlun – Bayan Har blocks (Meyer et al., 1998; Yin and Harrison, 2000; Tapponnier et al., 2001), at least in the western part of the range (Fig. 2c). The initiation age of deformation and uplift in the East Kunlun Range is still not fully constrained, estimations ranging from Eocene to Miocene (Mock et al., 1999; Jolivet et al., 2001; Clark et al., 2010; Duvall et al., 2013). Although probably limited in altitude (Wang et al., 2021), some pre-Paleocene reliefs are inferred in that region though the Qaidam Basin was still extending south, connecting to the Hoh Xil Basin on the Bayan Har terrane (Fig. 1) (Cheng et al., 2015b; Staisch et al., 2020). Tectonic uplift increased during the Oligocene and again during the Miocene (Jolivet et al., 2001; Duvall et al., 2013; Cheng et al., 2015b; Li et al., 2020). The total horizontal Cenozoic displacement along the central Kunlun fault is estimated at 100 ± 20 km (Kidd and Molnar, 1988; Fu and Awata, 2007). The structure of the range, and the associated topography is divided in three distinct domains: east of 94°E, the range is narrow (about 75 km wide), mainly controlled by the strike-slip Kunlun fault along its southern limit and the South Qaidam fault, a frontal thrust separating the range from the Qaidam Basin. This geometry, associated to the very limited width of the range suggest that southward subduction of the Qaidam lithopshere underneath the easternmost part of the East Kunlun range is still incipient and very limited (Fig. 2b). That assumption is further supported by wide-angle seismic data, some authors even suggesting northward motion of the East Kunlun lower crust below the Qaidam block (Karplus et al., 2019; 2011).

To the west, the Qimen Tagh ranges spread over more than 200 km in width, formed by a series of arcuate NW – SE sub-ranges developing along transpressive faults (Figs. 1a and 4a). The vergence of those faults has been largely discussed (Meyer et al., 1998; Jolivet et al., 2001; Yin et al., 2007a, 2008). and the debate remains open. Based on the interpretation of satellite images Meyer et al., (1998) proposed that the Qimen Tagh range developed as a north verging accretionary prism allowing the southward subduction of the Qaidam crust below the Kunlun – Bayan Har region (Fig. 1). Based on field mapping and seismic profile analysis, Yin et al. (2007a, 2008) proposed that the

Qimen Tagh is a south verging accretionary prism formed by wedging of the Kunlun crust between the Qaidam crust and the southward subducting Qaidam lithosphere. However, a recent model based on basin analysis, seismic data and analysis of satellite images proposed that the main Qimen Tagh faults be mostly north-verging, initiating as left-lateral strike-slip structures forming the western termination of the Kunlun fault (Cheng et al., 2014) (Fig. 2b). Miocene to present day northeastward displacement of the Qaidam block along the Altyn Tagh fault induced the progressive migration of the faults, increasing their compressive component. This migration seems further attested by the progressive northward propagation of the strike-slip Baiganhu (or Kadzi) fault since the middle Miocene as a transform fault, sub-parallel to the Altyn Tagh fault (Wu et al., 2020; Liu et al., 2021) (Fig. 4). Though the exact geometry of the Qimen Tagh ranges still remains to be documented, it corresponds to that of a wide basement-involved accretionary prism and suggest a well-developed southward subduction of the Qaidam block lithosphere underneath the Kunlun – Bayan Har blocks (Figs. 1A and 2c). Such a subduction may explain the formation of late Cenozoic crustal-derived magmas (shoshonites and rhyolite) on the northern edge of the Tibetan plateau in that region (Arnaud et al., 1992; Turner et al., 1996; Hacker et al., 2000; Jolivet et al., 2003). Some of these magmas include high-pressure granulite xenoliths indicating sampling depth of 50 to 60 km (14 to 17 kbars, 1000 to 1100°C) (Jolivet et al., 2003). This volcanism does not occur east of the Qimen Tagh region, further supporting the idea that continental subduction to the east is very limited.

Finally, west of the Baiganhu fault, the sigmoidal-shape Jianxia Shan thrust belt is formed by a series of stacked thrust faults. These accommodate both the strike-slip motion along the Altyn Tagh fault and NE-SW regional shortening (Wu et al., 2020) (Fig. 4).

Qilian Shan range

On the northeastern margin of the Tibetan plateau, the Qilian Shan is formed by a series of parallel sub-ranges extending over nearly 400 km in width between the Qaidam Basin and the North China

craton (Figs. 2b,c and 5). The crustal structure of the range inherited from a long and complex geodynamic history. The Proterozoic basement is affected by several Early to Middle Paleozoic suture zones marked by UHP rocks such as the North Qaidam eclogites at the limit between the Qaidam and Qilian Shan (Yang et al., 2000; Song et al., 2003; Yin et al., 2007b; Menold et al., 2009; Chen et al., 2012) or the North Qilian ophiolite separating the North Qilian Shan from the North China Block to the north (Song et al., 2009). Geophysical data indicate a significant downward inflection of the Moho below the range (Meng and Cui., 1997) and crustal-scale thrusts are inferred on the eastern front of the range (Wu et al., 1996). Recently acquired magnetotelluric and deep-seismic reflection data suggest that a south-verging (possibly bivergent) oceanic slab is preserved below the range, at least in the southern region (Chen et al., 2019; Huang et al., 2021, Li et al., 2021) (Fig. 2b). The presence of such a slab further north as suggested on Figure 2c remains highly speculative although geometrically coherent. Early Paleozoic metasedimentary series are extensively exposed throughout the range, unconformably covered by Permian and Triassic detrital series in the central region between Lake Hala and Lake Qinghai (Fig. 5). Early to Middle Jurassic sinistral strike-slip movement along the Altyn Tagh fault induced extension in the northern part of the Qilian Shan and tranpression further away from the fault, creating depocenters along the eastern margin of the Qaidam Basin and in the Hexi Corridor (Vincent and Allen., 1999). Rotation in the regional stress-field during the Late Jurassic – Early Cretaceous subsequently inverted those basins, creating topographic uplift (George et al., 2001; Sobel et al., 2001; Pan et al., 2013; Cheng et al., 2018, 2019a). Cenozoic deformation is considered to have initiated in the South Qilian Shan during the Paleogene (Yin et al., 2008; He et al., 2017; Wang et al., 2017; Cheng et al., 2019a) before propagating northward until reaching the Northern Qilian Shan front during the middle to late Miocene (Jolivet et al., 2001; Zheng et al., 2010, Geosphere, Bovet et al., 2009; Li et al., 2019). In the northern part of the range, contraction along thrust faults, associated to strike-slip motion along the Altyn Tagh fault, accommodate the northeastward motion of the Qaidam Basin (Meyer et al., 1998; Cheng et al., 2015a; Zuza et al., 2016) (Fig. 2c). The south-eastern region of the range is

further characterized by a number of large strike-slip faults such as the Haiyuan, Riyueshan and Elashan faults (Fig. 5) that accommodate the regional shortening through eastward displacement of crustal blocks (Cheng et al, 2015a, 2021). Incipient lithospheric subduction of the North China craton southward along the northern margin of the range has long been inferred (Meyer et al., 1998; Tapponnier et al., 2001; Yin et al., 2008), with recent support from geophysical studies (Ye et al., 2015; Huang et al., 2021)

Methods

The aim of this work is to describe the mode of crustal deformation in northern Tibet using tectonic, geomorphic and thermal pattern indicators.

Crustal deformation modes and general geomorphic response

In general, crustal deformation in compressional setting can be described by three main models: distributed shortening, block uplift and crustal buckling (Fig. 6). Distributed shortening implies deformation along a series of compressive, transpressive or strike-slip faults (e.g., Meyer et al., 1998). This first deformation mode allows accommodating a large amount of convergence. The associated topography displays highly heterogeneous relief and exhumation, localized within narrow regions directly linked to the faults. The main rivers are generally parallel to the uplifting sub-ranges, fed by secondary drains perpendicular to the ridges (Beaumont et al., 2000; Burbank and Anderson, 2001). One exception are the major rivers pre-existing the newly-formed topography that may cut across the uplifting ranges if their incision rate is high enough to compensate the uplift rate. In intracontinental collisional settings, and in the absence of underlying magmatic plume, homogeneous block uplift leading to plateau formation is produced by diffuse deformation (e.g., Dewey and Bird, 1970). Erosion leading to strong incision but limited exhumation is initially confined to the edges of the block while internal surfaces are preserved as plateaus (Jolivet et al., 2007; Vassallo et al., 2007). Incision then migrates inside the uplifted block through time. Crustal

buckling forms through layer-parallel shortening (Turcotte and Schubert, 1982) and leads to the development of antiformal basement domes associated to subsiding synformal basins (Burg et al., 1994; Burg and Podladchikov, 2000). Relief and exhumation in the incipient dome are limited. Rivers are flowing radially from the highest part of the dome with generally limited incision. Exhumation is limited to the highest part of the dome. However, depending on the thermal state and rheology of the lithosphere, when shortening increases, doming will be replaced by thrusting with major thrusts developing on each limb of the initial fold (Burg and Schmalholz, 2008). Ongoing deformation may lead to exhumation of the deep crust such as in the Damba dome on the southern termination of the Longmen Shan range (eastern Tibet) (Weller et al., 2013; Jolivet et al., 2015).

Apatite fission track thermochronology as indicator of amount and age of the denudation

Apatite fission track thermochronology (AFT) (Hurford and Green, 1983; Laslett et al., 1987; Gallagher 1995) has been widely used in northern Tibet to date the initiation of the deformation and evaluate exhumation rates on specific structures (e.g., Jolivet et al., 1999; 2001, 2003; George et al., 2001; Sobel et al., 2001; Duvall et al., 2013; Wu et al., 2020). However, the temperature range in which the method applies (about 120°C to 60°C, corresponding to a depth range of about 3 to 4 km for a geothermal gradient of ~30°C/km) does not allow describing in details the evolution of the surface topography and relief (Ehlers and Farley, 2003). Furthermore, for the same reason, the method poorly constrains horizontal deformation that usually does not generate exhumation. Only exhumation in large restraining bends or satellite thrusts associated to strike-slip faults with a large displacement can be described. Nonetheless AFT thermochronology provides highly valuable constrains on the age of the major exhumation events and, when enough data are available on a large area, of the regional exhumation pattern. Below we compiled the mean basement-rocks AFT ages available from the literature. The mean age integrates the whole thermal history of a sample

during its crossing of the 120°C – 60°C temperature range (e.g., Laslett et al., 1987; Green et al., 1989) and we thus used those data to characterize the large-scale exhumation pattern of northern Tibet (Fig. 1B) (Jolivet, 2017).

Slope mapping, regional topographic profiles and river-bed longitudinal profiles.

To distinguish between high and low topographic gradient areas, topographic slopes were calculated (Horn, 1981) using the Shuttle Radar Topography Mission (SRTM) 30 m digital elevation model and the Generic Mapping Tools (GMT) software (Smith and Wessel, 1990; Wessel and Smith, 1991). In this work, slope maps are especially used to reveal fragments of pre-Cenozoic planation surfaces preserved within the various ranges (e.g., Craddock et al., 2014; Morin et al., 2019) and to distinguish areas of strongly compressive deformation (Clark et al., 2006a,b) (Fig. 1B). The pre-Cenozoic planation surfaces were defined as low-slope areas, generally below 10° (indicative of low relief) developed in crystalline or metamorphic basement or pre-Cenozoic sediment series. Following this method, the planation can either be related to erosion (when developed in basement) or sedimentation although the surfaces always correspond to pre-Cenozoic flat areas, undeformed during the Cenozoic orogeny (Morin et al., 2019). Using the same approach, strongly compressive areas are defined as high-slope regions (generally above 40°).

To describe the large-scale topographic evolution along-strike of the main ranges, topographic swath profiles were also drawn based on the SRTM data and using the GMT software. To allow estimating lateral topographic variations in a given section of the ranges, each profile is composed of stacked individual parallel topographic profiles acquired every kilometer over a 20 km wide region with a 20 m elevation sampling frequency. To evaluate the impact of the stacking width on the profiles, similar profiles have been drawn along the same axis but with a 10 km stacking width (Fig. Sup. 1). The mean profiles do not differ significantly and only the dispersion envelope is reduced. Finally, river-bed longitudinal profiles were acquired from the SRTM DEM on major or

characteristic rivers from each range. Both detachment-limited rivers (incision rate is controlled by the mechanics of river incision into bedrock) and transport-limited rivers (rivers showing incision or aggradation at a rate controlled by the sediment discharge) (Whipple and Tucker, 2002) are represented. The shape of such profiles provides information on the equilibrium state of the rivers (Leopold et al., 1953; Whipple, 2004; Peyron and Royden, 2013; Wickert and Schildgen, 2019). This equilibrium depends on multiples parameters including bedrock lithology, water and clastic material input and channel slope. In this work we used river profiles as proxy of tectonic deformation (river slope, occurrence of knickpoints) and relative incision rates. The general structure of the drainage system also provides information on the large-scale topographic evolution pattern.

Finally, associating all the above-mentioned information should allow estimating the equilibrium state of the topography which provides indications on the style and rate of deformation. This equilibrium state is often categorized as steady state and non-steady state topography . A steady-state topography is defined by a landscape that maintains a stable shape and in which erosion compensates rock uplift (Kooi and Beaumont, 1996; Beaumont et al., 2000; Burbank and Anderson, 2001; Willet and Brandon, 2002). In the framework of northern Tibet this may generally corresponds to highly dissected topographies. On the contrary, regions where remnants of flat erosion surfaces are preserved in the ranges and deeply incised by rivers will be considered as non-steady state topographies (Fig. Sup. 2). However, the structural pattern, kinematic setting, topographic heritage and long-term climate evolution of northern Tibet most probably prevent reaching a near-steady state topography, even locally. Liu-Zeng et al. (2008) defined the concepts of “positive” topography (a region showing a positive correlation between relief and altitude and local slope and altitude) and “negative” topography (showing an inverse correlation between relief and slope). In that model, a strongly positive topography will correspond to rapidly deforming, fast-growing ranges (the distributed shortening mode) while a negative topography will correspond to an uplifted but poorly deformed plateau surface (the block uplift model). However, the crustal

buckling mode defined above does not fit into those two end-members as it implies low slopes and low relief at all elevations (Fig. 6). Clark et al. (2006) working on Eastern Tibet defined an "active" landscape as areas affected by deep river incision leading to increased erosion rates and sediment export. They oppose it to a "relict landscape" formed by poorly-incised surfaces generally situated in the upper part of the drainage system of major rivers. In the following discussion, we will use the terms of "positive" topography as defined by Liu-Zeng to characterize the areas affected by deep incision and devoid of preserved paleo-surface remnants, and the term of "relict landscape" to describe the topography of areas showing extensive preservation of paleo-surfaces. Note that the drainage system in those "relict landscape" may not be connected to a major fluvial system as in the initial definition of Clark et al. (2006).

Results

Low temperature thermochronology

Apatite fission track data are summarized on Fig. 1b. In the Altun Shan, AFT data indicate strong late Miocene exhumation in the western part of the range (mean AFT ages below 10 Ma) (Jolivet et al., 1999; 2001; Li et al., 2015; Wu et al., 2020). However, data are only available along the North Altyn Tagh thrust fault that controls the uplift of the frontal part of the range (Fig. 1). No data exist inside the massif. Exhumation remains stronger along the northern edge of the range but decreases eastward, with the poorly exhumed eastern part recording Mesozoic mean AFT ages (Jolivet et al., 1999, 2001; Sobel et al. 2001; Li et al., 2015). Wang et al. (2008) reported a 5.1 Ma age from the planation surface west of the Xorkol Basin but no precise analytical data are given and the sample location is close to a large active fault that could generate localized exhumation. To the east of the Jinyan Shan AFT ages are all Mesozoic, including an Early Jurassic age of 167 ± 15 Ma on the northern front of the range (Jolivet et al., 2001).

In the East Kunlun Shan, AFT data record a highly diachronous exhumation patterns (Jolivet et al., 2001, 2003; Wang et al., 2004; Wang et al., 2006; Yuan et al., 2006; Duvall et al., 2013; Feng et al., 2017; Liu et al., 2017; Wang et al., 2018; Staisch et al., 2020; Tian et al., 2020; Wu et al., 2020; Liu et al., 2021). Middle to Late Miocene ages indicate strong exhumation in the Jianxia Shan (Figs. 1 and 5). In contrast, immediately east of the Baiganhu fault (Fig. 5), in the Qimen Tagh ranges the widespread occurrence of Mesozoic to early Cenozoic ages indicate very limited exhumation. Miocene ages are only recorded along the main Kunlun fault and very locally on some of the major thrust faults (Jolivet et al., 2001, 2003; Liu et al., 2017). Further east, the Eastern Kunlun Shan display Mesozoic to early Cenozoic AFT ages associated to Oligocene to Pliocene ages along the major faults indicating that exhumation is not distributed but strongly localized along the major structures.

In the Qilian Shan, AFT data reveal an exhumation pattern largely controlled by the main thrust faults (Qi et al., 2016; Li et al., 2019) or very locally along major strike-slip fault such as the Haiyuan fault (Yu et al., 2019; Wu et al., 2021). The distribution of the AFT ages is similar to that of the Altyn Tagh and Kunlun, with a large number of Mesozoic (mainly Cretaceous) ages associated, near the faults to Oligocene and Miocene ages. However, the young, late Miocene to Pliocene ages observed in the western Altun Shan and central East Kunlun Shan are absent, suggesting low exhumation. However, it should be noticed that a large region between Lake Hala and the Altyn Tagh fault (including some of the highest summits) as well as some areas east of Lake Qinghai are not documented. The AFT ages tend to increase in the southeastward part of the range where only few Miocene ages are reported (Lease et al., 2011; Lu et al., 2012) among over-represented Mesozoic and Paleogene ages.

Range-scale geomorphology

The Altun Shan.

The range is arc-shaped, convex toward the Tarim Basin and limited by the Altyn Tagh fault to the south (Fig. 1a). Several large transpressive faults near-parallel to the Altyn Tagh fault divide the range into SW-NE elongated compartments (Fig. 2). The highest summits (up to about 6240 m) are situated in the western half of the range, along restraining bends directly linked to shearing along the Altyn Tagh fault. The western end of the Altun Shan range shows a high-relief, strongly dissected topography. A topographic profile perpendicular to the range in the westernmost area (profile Topo 1, Fig. 7) suggests that although dissected, the morphology north of the Altyn Tagh fault corresponds to a surface tilted northward toward the Tarim and offset by at least two major faults (F1 and F2 on figures 3 and 7). The fault that shows the largest vertical offset (F1) shows a southward normal topographic throw of about 1000 m. However, this offset may be overestimated has it is calculated using the mean value of the DEM elevation data which are very poorly resolved in that part of the range. River beds are narrow and largely free of clastic material (bedrock rivers). Although numerous no-data pixels are present in the SRTM elevation data, the river profiles in that region are concave without major knickpoint, suggesting that trunk channels are at near-equilibrium (Leopold and Maddok, 1953; Goldrick and Bishop, 2007; Robl et al., 2017) (profiles R1 and R2, Fig. 7). However, we acknowledge that existing knickpoints may be hidden by the strong pixel noise. The deep incision of narrow gorges and the generally very high slopes (Fig. 1) characterise a region of positive topography associated with strong deformation. However, it should be noted that the concavity decreases eastward from profile R1 to R2 forecasting a lateral change in topographic balance.

The magnitude of river incision decreases progressively eastward until the topography becomes characterized by a wide planation surface worn into the Proterozoic and Paleozoic crystalline basement. This erosion surface, is also affected by faults but the major throw observed to the west is not present (profile Topo 2, Fig. 7). The tilt of the surface is generally limited to a few degrees, the northern compartment, covered by Quaternary deposits (Liu, 1988) being horizontal. Only the northernmost part of the range shows strong slopes and incisions linked to uplift along the North

Altyn Tagh thrust fault (Fig. 3). Overall incision is limited to a few rivers flowing perpendicular to the range. In the southern part of the range, satellite images show that rivers are gravel-bedded with wide river beds. However, in the central (on the horizontal plateau) and northern areas, they form deep gorges with little detrital material preserved in the river bed. The trunk channels have a generally low-slope profile with two obvious knickpoints associated with major faults (profile R3, Fig. 7). The slope of the river bed decreases at the onset of the gorges (see river segment below point K2 on profile R3, Fig. 7). The topography of this part of the Altun Shan range thus appears to correspond largely to the relict landscape type, erosion being largely outpaced by tectonic uplift.

The central part of the range is mainly characterized by the transtensive Xorkol Basin (Fig. 3). To the south, the Akatengmeng Shan massif, although affected by a relay zone between two segments of the Altyn Tagh fault, displays a generally-flat north-dipping topography (profile Topo 3, Fig. 7). North of the Xorkol Basin, the Jinyan Shan massif (Fig. 3) again shows a flat mean topography, tilted to the north and split in two compartments by a major fault (F3 on Figs. 3 and 7) having a mean southward normal topographic throw of about 500 m. These offsets are consistent with the occurrence of large normal faults bordering the southern and north edges of the Xorkol Basin (Wang et al., 2008). Fragments of planation surfaces are preserved especially in the eastern part of the massif, supporting Eocene sediments, unconformably covered by Quaternary deposits (Liu, 1988; Li et al., 2018). In that part of the Altun Shan range, the water divide is located along the northern edge of the Xorkol Basin, and no river crosses the entire range. The rivers flowing northward across the Jinyan Shan are gravel-bedded with generally wide beds and display a very regular, slightly concave, profile (profile R4, Fig. 7). Being more complex due to the occurrence of the Xorkol Basin, this section of the Altun Shan corresponds mainly to a relict landscape associated to some local areas of positive topography along major faults (Fig. 1).

Finally, to the extreme east of the Altun Shan, the topography is complex and no individual surfaces can be clearly distinguished. The topography distributes into a general dome-like shape divided in three parts by two valleys (profile Topo 4, Fig. 7). Incision is distributed among many small drains,

controlled by the numerous en-échelon thrust faults that are merging with the main Altyn Tagh fault. Rivers flowing north have a regular, poorly concave profile similar to those of the Jinyan Shan (profile R5, Fig. 7). This topography is again largely associated to the relict landscape type.

The East Kunlun Shan

In the eastern part of the East Kunlun range, river incision is important and except for those flowing along the Kunlun fault valley, most rivers are flowing northward, perpendicular to the range (Fig. 4). Transverse topographic profiles display a steep frontal relief along the thrust fault separating the Qaidam Basin from the range (profiles Topo 1 and Topo 2, Fig. 8). This initial step in the topography is followed by a topographic compartment with altitudes varying between about 4000 m and slightly less than 5000 m, showing several large fragments of flat surfaces at altitudes above 4500 m and mainly worn into Permian-Triassic granites or Proterozoic gneisses (Clark et al., 2010; Li et al., 2021) (Fig. 4). Some of these surfaces display deep incisions although the rivers mostly remain gravel-bedded. The Nuomuhong river (river R1, Fig. 8), flowing perpendicular to the range immediately east of one of the major planation surfaces, show as slightly concave, relatively steep profile with a potential knickpoint in its upper part. Further west, the Golmud river (river R2, Fig. 8) that flows parallel to the range before crossing it has a regular, low-slope profile, slightly convex in its upper part, without knickpoints. The low-slope profile suggests a limited sediment-to-water discharge ratio (Wickert and Schildgen, 2019). The river incises in its own alluvium along most of its length which might be related either-to or to a combination of an increase in water discharge (Poisson et al., 2004), a drop in base level due to Late Pleistocene drying of the Qarhan palaeo-lake system forming the base level in the Qaidam Basin (An et al., 2012) or an increase in tectonic uplift rates. Finally, river R3 (Fig. 8) flows perpendicular to the range in a poorly incised, low slope surface at the limit between the eastern East Kunlun range and the Qimen Tagh. The river profile is similar to that of the Nuomuhong river, with at least one marked knickpoint in its upper reaches and

probably a second downstream. Based on satellite images, the river bed seems to contain less sediment than the other rivers as bedrock is visible at least in the section between the two knickpoints. Both knickpoints correspond to faults affecting the surface. All three river profiles appear out of equilibrium. In general, this topography can be categorized as a relict landscape: tectonic uplift seems to outpace erosion as attested by knickpoints, Mesozoic to Paleogene AFT ages (Fig. 1B) and ancient erosion surfaces largely preserved at high altitude. However, the deep incision and higher exhumation in the frontal part of the range and along the major strike-slip faults as attested by late Cenozoic AFT ages indicate a transition toward active topography.

The topography of the Qimen Tagh is completely different (Fig. 4). As indicated above, the range widens rapidly, the topography including narrow thrust-controlled ranges separated by wide basins filled with Eocene to Quaternary clastic sediments to the east and mostly Neogene to Quaternary deposits to the west (Liu, 1988). Those basins host lakes in their western part, that form local base levels for the rivers, making for a complex series of non-connected ranges-parallel drainage sub-systems. All the main rivers flow NW suggesting a general slope in that direction, fitting with the presence of the lakes to the west. River profile R4 (Fig. 8) represents a characteristic example of one of those rivers although it crosses the northern sub-range to connect to Lake Gaskule in the SW Qaidam Basin (Fig. 4). From satellite images observation, the river bed is wide, full of sediment and shows only a very limited incision. The longitudinal profile is regular with a relatively low slope. These two observations suggest limited tectonic disturbance of the river profile, even on crossing the frontal range, and a low sediment-to-water discharge ratio (Wickert and Schildgen, 2019). The topographic profiles across the range indicate a progressive decrease of the relief from east to west (profiles Topo 3 to Topo 5, Fig. 8), consistent with the general low exhumation indicated by the AFT data. Part of that decrease in relief is linked to sedimentation in the multiple isolated basins. All these observations complemented by the Mesozoic and Paleogene AFT ages (Fig. 1b) suggest a relict landscape type topography associated with localized positive topography along the major thrust faults.

Finally, the Jianxia Shan displays a highly dissected, positive topography very similar to that of the westernmost part of the Altun Shan (Fig. 4). Most rivers are bedrock channels. This is consistent with the recent and strong exhumation suggested by the Middle to Late Miocene AFT ages reported in that region (Wu et al., 2020).

The Qilian Shan

Groves et al. (2020) recently investigated the large scale-geomorphology of the Qilian Shan and divided the range in 5 different domains based on the distribution of geomorphic indexes. Below we simplified this division to three main zones (Fig. 5). From the Altyn Tagh fault to Lake Hala, the topography is composed of a series of narrow, high ranges separated by sedimentary basins (profile Topo 1, Fig. 9). The width of those ranges increases eastward while their altitude increases toward the axial part of the range before decreasing again eastward. The relief of the sub-ranges are steep with strong incision (Fig. 1b). However, some limited-relief basement surfaces are preserved, especially a large one in the Sule Nan Shan (Figs. 5 and 9). The main rivers that flow in that part of the range are gravel-bedded drains, largely parallel to the ranges, similar to those of the Qimen Tagh. All the main rivers are flowing north toward the Altyn Tagh fault, suggesting again a general slope in that direction. Except for those flowing into Lake Suhai that forms a local base level in the Suganhu Basin, the rivers are crossing the Altyn Tagh fault to reach the regional base level formed by the much lower Tarim Basin. The Danghewan River (river R1, Fig. 9) flows from the southern summits of the Sule Nan Shan along the eastern side of the Tang He Nan Shan before crossing the Altyn Tagh fault. The upper part of the river profile is marked by a typical concave shape with possibly a first knickpoint on reaching the intra-mountain basin. The lower part of the profile is characterized by two well-marked knickpoints on crossing the ranges associated to the Altyn Tagh fault. Except for some limited bedrock-confined segments, the Changma River (river R2, Fig. 9) is also gravel-bedded. Sourced on a mountain ridge separating Lake Hala basin from Lake Qinghai

drainage area, it flows inside the Ta Shue Shan sub-range, parallel to the range axis before crossing it and the northern tip of the Qilian Shan sub-range northward to reach the eastern tip of the Altyn Tagh fault. On reaching the Tarim Basin it forms a huge alluvial fan. The river profile is flat, slightly convex in its upper-central part suggesting that rock uplift in the Ta Shue Shan (Fig. 5) is not equilibrated by river incision. The fact that the river crosses the Ta Shue Shan and Qilian Shan sub-ranges instead of being guided along-strike, suggests that it was antecedent to the ranges and was able to incise fast-enough to compensate uplift. No knickpoint is observed on crossing the Altyn Tagh fault, indicating that river incision largely compensates the tectonic uplift. The topography of that region is categorized as positive topography although it is largely smoothed by sediment deposits in-between the main sub-ranges (Liu-Zeng et al., 2008). However, it is interesting to note that although the topography has been largely reworked by recent tectonics, part of the drainage system seems to be inherited from a previous landscape.

A topographic profile immediately north of Lake Hala displays a general dome-like shape of the range, the lake being situated on the top of the dome (profile Topo 2, Figs. 5 and 8). The range is still formed by a series of parallel sub-ranges but their relief is lower than to the north except along the eastern front of the range marked by a sharp 3000 m drop in altitude on reaching the Hexi Corridor (Figs. 1A and 5). Large fragments of low-relief erosion surfaces are exposed in that region, including a huge surface between Lake Hala and the Qaidam Basin (Fig. 5b). South of Lake Hala, in the northern part of Lake Qinghai drainage area, the width of the range decreases and the dome-like shape is well-expressed in the central part, bordered by the high-relief of the Qilian Shan to the east and the Delingha Basin (Fig. 5) to the west (profile Topo 3, Fig. 9). A major part of the topography in the central part of that region is formed by poorly-incised surfaces (Fig. 5c). It includes the most extensive, flat-lying Permian and Triassic outcrops within the whole range. AFT mean ages are mostly Upper Cretaceous to Paleocene in the central region while available Neogene ages are restricted to the front of the Qinghai Nan Shan and to the vicinity of the Haiyuan fault (Lu et al., 2012; Qi et al., 2016) (Fig. 1b). This region is the source of many rivers diverging radially

from the summit of the dome (including the Changma River described above). The Xiala-Heihe River is flowing eastward across the Qilian Shan (river R3, Fig. 9) and shows a relatively steep-slope profile with no or poorly marked knickpoints suggesting a relative equilibrium between uplift and incision (note that the lower part of the profile is disturbed by the occurrence of a dam lake). The Buha River initiates in the same region but flows the opposite way toward Lake Qinghai with a constant, low-slope profile (river R4, Fig. 9). This reflects the low slopes prevailing in that region as the river mostly flows across the poorly incised surface supporting the Permian – Triassic series. The topography of that region is clearly of relict landscape type except for the northern front of the range where positive topography dominates.

South of Lake Qinghai, the range narrows again down to about 250 km instead of 350 km north of Lake Hala. The dome-like shape observed in the previous profiles is no more present (profile Topo 4, Fig. 9). The topography is formed by a series of sub-ranges separated by narrow valleys and most rivers are flowing toward the SE. Incision is stronger, including the deep Longyang Gorge formed by the Yellow River (Lin et al., 2021 and references therein). Several low-relief erosion surfaces are preserved in that region but not to the extend observed further north (Craddock et al., 2014; Lin et al., 2021). AFT mean ages are widely spread between Lower Jurassic (Lin et al., 2021) and Eocene ages (Wang et al., 2016) (Fig. 1b). No Neogene ages are reported indicating a generally low Cenozoic exhumation although exhumation initiated around Late Miocene along the western front of the range (Craddock et al., 2014) and Middle to Late Miocene along the eastern front (Li et al., 2019). Once again, the topography seems intermediate between a relict landscape type and a newly developing positive topography type.

Discussion

The geomorphic analysis presented above demonstrate that the deformation pattern varies largely from one-another and inside the individual ranges that form the northern edge of the Tibetan plateau. After discussing and comparing the deformation in each range, we propose a synthetic model showing that the three main modes of deformation described above occur simultaneously in northern Tibet: 1) distributed shortening, 2) homogeneous block uplift and 3) crustal buckling.

Below we first discuss the occurrence of these three types of deformation in northern Tibet. We then show that their distribution suggests the occurrence of a transition zone, traversing across the central parts of the East Kunlun range, the Qaidam Basin and the Qilian Shan, parallel to the Altyn Tagh fault.

Deformation pattern within individual ranges.

The topography of the Altun Shan range corresponds to an ancient planation surface (probably of Early Mesozoic age (Jolivet, 2017)) tilted northward along major normal faults and eastward as a general trend (Figs. 1 and 3). The strongly positive topography and Pliocene AFT ages in the western part of the range attest of recent strong deformation and exhumation. However, except in this westernmost part, exhumation is low to very low as evidenced by the widely distributed Mesozoic and early Cenozoic AFT ages (Fig. 1b). The topography is mainly of relict landscape type showing a relief largely in disequilibrium as incision does not compensate uplift. Wang et al. (2008) proposed that the Altyn Tagh range is a restraining bend along the Altyn Tagh fault, with extension in the Xorkol Basin being related to oroclinal bending. However, such a model would require that, before extension takes place in the central part of the growing dome, exhumation should be important as observed in the smaller-scale restraining bends such as the Akato Tagh (Fig. 3) (Cowgill et al., 2004a,b). This is not recorded in the topography that preserved flat paleo-surfaces nor in the low temperature thermochronology data. The only area where doming might be suggested is the eastern-most part of the range (see profile Topo 4, Fig. 7). We propose that the Altyn Tagh

range corresponds to a narrow, basement involved accretionary prism accommodating the subduction of the Tarim lithosphere beneath the Qaidam and Kunlun blocks (Fig. 2a).

Although they represent the present-day deformation pattern and should be extrapolated back in time with caution, global positioning system (GPS) measurements of crustal motion available in the western part of the range indicate north-directed displacements (relative to a fixed Eurasian Plate reference), at a high angle to the faults (Calais et al., 2006; Gan et al., 2007; Wang and Shen, 2019) (Fig. 1a). The general uplift of the range is controlled by the steep frontal thrusts such as the North Altyn Tagh fault that decouple the subducting and shortening Tarim crust from northern Tibet. To the south, the nearly purely strike-slip Altyn Tagh fault acts as a backstop structure to the Altun Shan terrane, decoupling it from the Qaidam and Kunlun blocks. The deformation of the upper crust in the Altyn Tagh range is thus accommodated by thrusting on the frontal North Altyn Tagh fault and transtensive movements leading to the formation of pull-apart basins along southward verging faults inherited from the Mesozoic transtensional phase (Chen et al., 2003; Cheng et al., 2019a; Zhao et al., 2020). This structural pattern leads to vertical uplift of crustal blocks with only limited shortening to the west (most probably driven by the general sinistral component affecting the range), preserving the initial surface from deformation. The dry climate (less than 250 mm.yr-1 precipitation (Hong et al., 2005)) associated to low slopes and recent onset of uplift, explains the limited incision and the highly unbalanced topography. Only to the east, where, as suggested by the available GPS data, the strike of the faults favors strike-slip motion, oroclinal bending may occur.

In the eastern part of the East Kunlun Shan, the GPS data indicate a nearly 45° angle between the direction of crustal motion and the strike of major faults (Fig. 1a). The range is narrow (about 80 km wide) and the deformation linked to the southward subduction of the Qaidam lithosphere is mainly accommodated by partitioning along the strike-slip Kunlun fault as well as on a near-unique frontal, steeply dipping South Qaidam thrust fault (Figs. 4 and 2b). As indicated by the occurrence of late Cenozoic AFT ages), exhumation is localized in the restraining bends along the strike-slip

fault (Jolivet et al., 2001, 2003; Wang et al., 2006) and the major rivers are incising deeply in the range indicating strong regional rock uplift. However, in general the topography is of relict landscape type and, as attested by the Mesozoic and early Cenozoic AFT ages, regional exhumation remains limited, preserving large fragments of the Mesozoic erosion surface (Clark et al., 2010; Roger et al., 2011; Duvall et al., 2013; Jolivet, 2017; Li et al., 2021). The setting is largely similar to that of the central Altun Shan. To the west, in the Qimen Tagh, the deformation pattern is controlled by strike-slip motion along both the Kunlun and Altyn Tagh faults as demonstrated by Cheng et al. (2014, 2015a). The deformation is highly localized along major – basement involved – thrust faults that propagate into the SW Qaidam Basin, most probably along a mid-crustal décollement level (Meyer et al., 1998) (Fig. 2c). The GPS data indicate a crustal motion near perpendicular to the strike of the faults, suggesting the absence of strike-slip component on those structures (Fig. 1a). However, seismic imaging analysis and river bed lateral shifts have revealed the occurrence of a noticeable strike-slip component on several of those faults (Cheng et al., 2014, 2015b). The Qimen Tagh thrusts are widely spread on a total range-width of about 200 km which makes for an overall limited relief and exhumation as indicated by the low temperature thermochronology data (Fig. 1b). Because the deformation is localized, sub-ranges are narrow, impeding internal preservation of the Mesozoic planation surface. However, those surfaces are probably preserved between the ranges as suggested by the general low exhumation, implying that the large-scale topography is mostly of relict landscape type but includes positive topography in the narrow ranges.

As recently demonstrated by Allen et al. (2017) and Groves et al. (2020) the topography of the Qilian Shan evolves from SE to NW. South of the southeastern tip of the Qaidam basin, the range is narrower and, as suggested by the AFT data, the topography is largely inherited from a Cretaceous exhumation event (e.g., Lu et al., 2012; Li et al., 2019, 2020; Lin et al., 2021; Wang et al., 2021) (Figs. 1b and 5). In that region, the GPS data indicate crustal motion at a relatively low angle to the

main faults strike, as attested by the strong strike-slip component along many of those faults. This major horizontal component limits the exhumation to a few restraining bends and thrust faults (Lin et al., 2021; Lease et al., 2011). Between Lake Qinghai and Lake Hala, the GPS displacement data show vectors near perpendicular to the strike of the faults, implying pure shortening (Fig. 1b). The topography largely preserved the Mesozoic surface, with very limited Cenozoic deformation and associated exhumation as attested by the large preservation of Permian to Triassic series and the Late Cretaceous to Paleocene AFT mean ages (Figs. 1b and 2b). Active thrusts are restricted to the edges of the range and Allen et al. (2017) described this area as similar to the initial Tibetan plateau. The region includes the source of many of the large rivers flowing through the range in a diverging pattern (Fig. 5). Meng et al. (2020) suggested that this river pattern resulted from a Late Miocene complete re-organization of the river network linked to the onset of strike-slip motion along the Haiyuan fault. However, their model suggests that rivers flow parallel to major thrusts. While this is largely the case in the northern region, it is not true for the central and southern regions. The topographic profiles reported in this work suggest that the plateau-like topography observed in the central part of the Qilian Shan accommodates deformation through doming (Fig. 9). Lake Hala Basin marks a major limit: to the north, the topography is composed of a series of parallel sub-ranges developing on major thrust faults and separated by wide valleys (Fig. 2c). The uplift of the sub-ranges is largely controlled by strike-slip motion along the Altyn Tagh (Allen et al., 2017), in a similar way to the northward migration of the Qimen Tagh thrusts. However, the Paleozoic suture zones located in the Danghe Nanshan and the Daxue Shan and the contrasted basement-block lithology probably impede the development of a single, continuous crustal décollement level previously suggested by Meyer et al. (1998) (Fig. 2c). Few AFT ages are available inside this part of the Qilian Shan but the observation that some of the main rivers that cut across subranges may be inherited from a previous drainage network, suggest that the topography still contains some relict geomorphic elements.

Large-scale deformation pattern in northern Tibet: coexisting deformation modes

The three modes of deformation described above appear to coexist in northern Tibet: block uplift, distributed shortening and crustal buckling (Fig. 2). Below we propose a crustal-scale model of the deformation in northern Tibet, taking into account both the regional structural pattern and the surface morphology (Fig. 10).

Deformation is strongly partitioned across the lithospheric-scale Altyn Tagh fault. In the southern part of the Altun Shan, shortening and incipient subduction of the Tarim crust below the Qaidam block is accommodated by strike-slip NE-SW transpressive and ESE-WNW transtensive faults. However, some of the deformation is also accommodated along the steep frontal North Altyn Tagh thrust fault and, to a limited extend on the Tanan rise system immediately to the north (Fig. 1 and 2a). This structural pattern leads to a near-homogeneous uplift and northeastward tilting of the Altun Shan block.

Immediately south-southeast of the Altyn Tagh fault, the Cenozoic NE-SW shortening of northern Tibet is accommodated by a large accretionary prism encompassing the Kunlun, the NW Qaidam Basin and the South Qilian Shan. NW-SE parallel thrusts, formed as en échelon thrusts accompanying the strike-slip motion, develop at a high angle to the main Altyn Tagh fault (Figs. 1a and 2c). This angle increases eastward from about 40° in the Qimen Tagh to 55° for the folds and thrusts in the north Qaidam Basin and 60° in the Qilian Shan. The increasing angle is correlated to a clockwise rotation in the direction of crustal motion as observed from GPS data (Zuza and Yin, 2016; Wang et al., 2019; Cheng et al., 2021) (Fig. 1b). Separating the South Qilian Shan block from the Central Qilian Shan block, the Danghe Nanshan thrust system presents some of the highest slopes, altitudes and denudation rates inside the thrust system (Fig. 1b and profile Topo 1, Fig. 9). It is a major system associating thrusting and sinistral strike-slip (Meyer et al., 1998). Similarly, the Daxue Shan thrust system is superposed to the north Qilian Shan suture zone and again displays steep slopes and high altitudes. Finally, the North Qilian Shan sub-belt extending along the whole

eastern front of the range displays the strongest observed topographic gradients (Figs. 1b and 9) (Allen et al., 2017; Groves et al., 2020; Meng et al., 2020). As already suggested (Meyer et al., 1998; Tapponnier et al., 2001; Cheng et al., 2019b), the Central Qilian Shan block – limited by the two weak zones formed by the Paleozoic suture zones – may act as a backstop to the development of a second accretionary prism propagating eastward in the North China Block in response to the incipient subduction of that block beneath the Central Qilian Shan (Fig. 2c). As mentioned above, the occurrence of a Paleozoic oceanic slab below the Central and North Qilian Shan is highly speculative. However, magnetic anomaly data from the EMAG2v3 grid (calculate at 4 km altitude, Meyer et al., 2017) display a large, long-wavelength NW-SE negative anomaly below the Central and Northern Qilian Shan that might reflect the occurrence of a deep body (Fig. 11) (Kang et al., 2012).

To the west, between the Altyn Tagh fault and the Qimen Tagh, the Jianxia Shan is a fast-exhuming wedge-like structure between the Altyn Tagh fault and the Baiganhu fault. Crustal material is forced into the corner formed by the two faults, leading to rapid exhumation (Wu et al., 2020).

South-east of a limit running from the eastern tip of the Qimen Tagh to Lake Hala, the GPS data indicate crustal motion near perpendicular to the main tectonic structures. The deformation mode changes to vertical block uplift in the East Kunlun and crustal buckling in the Qilian Shan. Sedimentation and subsidence occur in the SE Qaidam Basin where shortening is only accommodated by a few folds (Yin et al., 2007, 2008). Wang et al. (2021) suggested downward crustal flexure as a subsidence mechanism for that part of the basin. The axial direction of the basin varies from about N130E north of the supposed limit to N100E to the south. It should also be noted that the first Cenozoic deposits in the Qaidam Basin (Lulehe to Lower Xaiganchaigou fms.) are largely restricted to the NW part (Yin et al., 2008; Cheng et al., 2018). This suggests that subsidence initiated first in the northern part of the basin (in relation with strike-slip movement on the Altyn Tagh fault) before crustal buckling initiated to the SE. Major thrusting, associated to high-relief is only limited to the eastern edge of the Qilian Shan, between the Haiyuan fault and the Hexi

Corridor (Fig. 2b). We suggest that the Haiyuan fault, largely superposed to the central Qilian Shan Paleozoic suture zone, plays a similar role as the Danghe Nanshan thrust system in segmenting the structural pattern of the range (Figs. 2b and 10).

Compiling the initiation ages of the major faults in northern Tibet, Duvall et al. (2013) divided the regional deformation history in two periods: prior to 20 Ma mostly in the Altyn Tagh realm to the NW and after 20 Ma in the region from the East Kunlun to the Haiyuan fault zone as well as, to some extend in the extreme NE Qilian Shan (see Figure 10 of Duvall et al., 2013). They relate this southeastward propagation of the deformation to the initiation of the Haiyuan fault. Although they include the frontal thrust of the East Kunlun Shan, near Golmud, into the pre-20 Ma fault pattern, the limit they suggest between the two sets of faults is similar to the limit defined between the deformation modes in this work. On surface, no obvious geological or structural feature directly fit with the proposed limit. However, EMAG2v3 magnetic data display a negative W-E anomaly connecting the eastern tip of the Qimen Tagh range to the large NW-SE negative anomaly in Lake Hala region (Fig. 11). This limit also corresponds to the limit between the numerous folds and faults accommodating the deformation in the western Qaidam and the few folds observed in the eastern part of the basin (Fig. 1a). This inferred shear zone would be parallel to the Altyn Tagh fault and ends to the east nearby the northern tip of the Haiyuan fault (Fig. 10). Te structure would accommodate the differential movement between the intracontinental subduction of the Qaidam lithosphere in the Qimen Tagh area and the absence of such subduction (collision) in the Eastern Kulun Shan (Fig. 10). The individualized SE Qaidam-South Qilian Shan block would accommodate deformation through crustal buckling but also southeastward motion along the East Kunlun – Haiyuan faults system and clockwise rotation.

If a strike-slip structure exists across the Qaidam Basin, many questions still remain to be addressed. For example, the deformation in the Qimen Tagh ranges, dated to the early Miocene (Cheng et al., 2014), marks the onset of the intracontinental subduction in that region. The onset of movement on the inferred lithospheric fault might thus be dated to the early – middle Miocene and

have accommodated several 10s of kilometers of strike-slip displacement. Such a displacement on a single fault should be expressed on the surface which is not the case. However, a wide, distributed shear zone may accommodate such amount of strike-slip movement at depth without obvious surface expression. Similarly, the occurrence of a large detachment fault in the lower to middle crust of the Qaidam Basin as suggested by several authors (e.g., Meyer et al., 1998; Yin et al., 2007, 2008) may distribute some of that deformation at depth.

Conclusions

The large-scale geomorphic analysis presented in this work, associated to the exhumation pattern derived from apatite fission track thermochronology suggest the occurrence of three different deformation modes in northern Tibet. The distributed shortening mode observed in the Qimen Tagh, north Qaidam Basin and north Qilian Shan is directly related to strike-slip motion along the Altyn Tagh fault and may represent the oldest, pre-Miocene deformation. To the SE, deformation appears largely accommodated by crustal buckling in the Qilian Shan and southern Qaidam Basin, as well as vertical block uplift in the East Kunlun Shan. Although it is poorly expressed as a geomorphic structure, an incipient shear zone running from the eastern tip of the Qimen Tagh range to the Haiyuan fault mays accommodate the differential movement between the intra-continental subduction to the NW and the collision in the Eastern Kunlun Shan. The existence of this inferred structure should be further documented by fieldwork in the Qilian Shan, especially SE of Lake Hala Basin.

Acknowledgements

We are grateful to An Yin, a anonymous reviewer and the Editor Kurt Sundell for their constructive comments on the initial version of this work.

References

ALLEN, M.B., WALTERS, R.J., SONG SHUGUANG, SAVILLE, CH., DE PAOLA, N., FORD, J., HU ZHENXING, & SUN WENLI. 2017. Partitioning of oblique convergence coupled to the fault locking behavior of fold-and-thrust belts: Evidence from the Qilian Shan, northeastern Tibetan Plateau. *Tectonics*, **36**, doi:10.1002/2017TC004476.

AN FU-YUAN, MA HAI-ZHOU, WEI HAI-CHENG, & LAI ZHONG-PING. 2012. Distinguishing aeolian signature from lacustrine sediments of the Qaidam Basin in northeastern Qinghai-Tibetan Plateau and its paleoclimatic implications. *Aeolian Research*, **4**, 17-30.

ARNAUD, N.O., VIDAL, P., TAPPONNIER, P., MATTE, P., & DENG, W.M. 1992. The high K2O volcanism of northwestern Tibet; geochemistry and tectonic implications. *Earth and Planetary Science Letters*, **111**, 351-367.

BEAUMONT, Ch., KOOI, H., & WILLETT, S. 2001. Coupled tectonic-surface process models with applications to rifted margins and collisional orogens. In SUMMERFIELD, M.A., (Ed.) Geomorphology and Global Tectonics, Wiley, Chichester, England, 367p.

BOVET, P.M., RITTS, B.D., GEHRELS, G., ABBINK, A.O., DARBY, B., & HOURIGAN, J. 2009. Evidence of Miocene crustal shortening in the north Qilian Shan from Cenozoic stratigraphy of the western Hexi Corridor, Gansu Province, China. *American Journal of Sciences*, **309**, 290–329. https:// doi.org/10.2475/00.4009.02.

BURBANK, D.W., & ANDERSON, R.S. 2001. Tectonic Geomorphology. Blackwell Science, 274 p., Malden, USA.

BURG J.P., DAVY P., AND MARTINOD J. 1994. Shortening of analogue models of the continental lithosphere : new hypothesis for the formation of the tibetan plateau. *Tectonics*, **13**, 475-483.

BURG, J.P., & PODLADCHIKOV Y. 2000. From buckling to asymmetric folding of the continental lithopshere: numerical modelling and application to the Himalayan syntaxes. In, KHAN, M.A., TREOLAR, P.J., SEARLE, M.P., & JAN, M.Q. (eds) *Tectonics of the*

Nanga Parbat Syntaxis and the Western Himalaya. *Geological Society, London, Special Publications*, **170**, 219-236.

BURG, J.P., & SCHMALHOLZ, S.M. 2008. Viscous heating allows thrusting to overcome crustal-scale buckling: Numerical investigation with application to the Himalayan syntaxes. *Earth and Planetary Science Letters*, **274**, 189-203.

CALAIS, E., DONG, L., WANG, M., SHEN, Z., & VERGNOLLE, M. 2006. Continental deformation in Asia from a combined GPS solution. *Geophysical Research Letters*, **33**, L24319, doi :10.1029/2006GL028433.

CHANG, H., LI, L., QIANG, X., GARZIONE, C.N., PULLEN, A. & AN, Z.. 2015. Magnetostratigraphy of Cenozoic deposits in the western Qaidam Basin and its implication for the surface uplift of the northeastern margin of the Tibetan Plateau. *Earth and Planetary Science Letters*, **430**, 271-283.

CHEN DAN-LING, LIU LIANG, SUN YONG, SUN WEI-DONG, ZHU XIAO-HUI, LIU XIAO-MING, & GUO CAI-LIAN. 2012. Felsic veins within UHP eclogite at Xitieshan in North Qaidam, NW China: Partial melting during exhumation. *Lithos*, **136-139**, 187-200.

CHEN, X., YIN, A., GEHRELS, G.E., COWGILL, E.S., GROVE, M., HARRISON, T.M., & WANG, X.F. 2003. Two phases of Mesozoic north-south extension in the eastern Altyn Tagh range, northern Tibetan Plateau. *Tectonics*, **22**, 1053, doi:10.1029/2001TC001336, 2003.

CHEN, X., SHAO, Z., XIONG, X., GAO, R., LIU, X., WANG, C., LI, B., WANG, Z., & ZHANG, Y. 2019. Fault system, deep structure and tectonic evolution of the Qilian Orogenic Belt, Northwest China. *Geology of China* (in Chinese with English abstract), **46**, 995–1020. doi:10.12029/gc20190504.

CHEN, Z., WANG, X., YIN, A., CHEN, B., & CHEN, X. 2004. Cenozoic left- slip motion along the central Altyn Tagh fault as inferred from the sedi- mentary record. *International Geology Review*, **46**, 839–856, doi: 10.2747/0020-6814.46.9.839.

CHENG, F., JOLIVET, M., FU ,S., ZHANG, Q., GUAN, S., YU, X., & GUO, Z. 2014. Northward rotation of the western East Kunlun Fault: Implications for the Late Cenozoic evolution of the Qimen Tagh Range and southwestern Qaidam Basin. *Tectonophysics*, **632**, 32-47.

CHENG, F., GUO, Z., JENKINS, H.S., FU, S., & CHENG, X. 2015a. Initial rupture and displacement on the Altyn Tagh fault, northern Tibetan Plateau: Constraints based on residual Mesozoic to Cenozoic strata in the western Qaidam Basin. *Geosphere*, **11**, 921-942.

CHENG, F., JOLIVET, M., DUPONT-NIVET, G., WANG, L., YU, X., & GUO, Z. 2015b. Lateral extrusion along the Altyn Tagh fault, Qilian Shan (NE Tibet): insight from 3D crustal budget. *Terra Nova*, **27**, 416-425.

CHENG, F., FU, S., JOLIVET, M., ZHANG, C., & GUO, Z. 2015c. Cenozoic basin-range interactions in the southwestern Qaidam Basin: Constrains from detrital U-Pb zircon geochronology and sedimentology. *Geological Society of America Bulletin*, doi:10.1130/B31260.1.

CHENG, F., JOLIVET, M., GUO, ZH., FU, S., ZHANG, CH., & ZHANG, Q. 2016. Large-scale displacement along the Altyn Tagh Fault (North Tibet) since its Eocene initiation: Insight from detrital zircon U-Pb geochronology and subsurface data. *Tectonophysics*, **677-67**8, 261-279.

CHENG FENG, JOLIVET, M., HALLOT, E., DAOWEI ZHANG, CHANGHAO ZHANG & GUO ZHAOJIE. 2017. Tectono-magmatic rejuvenation of the Qaidam craton, northern Tibet. *Gondwana Research*, **49**, 248-263.

CHENG FENG, GARZIONE, C., JOLIVET, M., WEITAO WANG, JIBAO DONG, RICHTER, F. & GUO ZHAOJIE. 2018. Provenance analysis of the Yumen Basin and northern Qilian Shan: Implications for the pre-collisional paleogeography in the NE Tibetan plateau and eastern termination of Altyn Tagh fault. *Gondwana Research*, **65**, 156-171.

CHENG FENG, JOLIVET, M., GUO ZHAOJIE, LU HUAYU, ZHANG BO, LI XIANGZHONG, ZHANG DAOWEI, ZHANG CHANGHAO, ZHANG HANZHI, & ZHANG QIQUAN. 2019a. Jurassic- Early Cenozoic tectonic inversion in the Qilian Shan and Qaidam Basin,

North Tibet: new insights from seismic reflection, isopach mapping and drill core data. *Journal of Geophysical Research – Solid Earth*, **124**. https://doi.org/10.1029/2019JB018086.

CHENG FENG, GARZIONE, C.N., MITRA, G., JOLIVET, M., GUO ZHOAJIE, LU HUAYU, LI XIANGZHONG, ZHANG BO, ZHANG DAOWEI, ZHANG CHANGHAO, ZHANG HANZI, & ZHANG QIQUAN. 2019b. The interplay between climate and tectonics during the upward and outward growth of the Qilian Shan orogenic wedge, northern Tibetan Plateau. *Earth-Science Reviews*, **198**, https://doi.org/10.1016/j.earscirev.2019.102945

CHENG, F., JOLIVET, M., GUO, ZH., ZHANG ,CH., ZHANG, Q., & LI X. 2021a. Cenozoic evolution of the Qaidam Basin and implications for the growth of the northern Tibetan plateau: A review. *Earth Science Reviews*, in press.

CHENG, F., ZUZA, A.V., HAPROFF, P.J., WU, C., NEUDORF, C., CHANG, H., LI, X., & LI, B. 2021. Accommodation of India–Asia convergence via strike-slip faulting and block rotation in the Qilian Shan fold–thrust belt, northern margin of the Tibetan Plateau. *Journal of the Geological Society*, jgs2020-2207.

CLARK, M.K., ROYDEN, L.H., WHIPPLE K.X., BURCHFIELD, B.C., ZHANG, X., & TANG, W. 2006a. Use of a regional, relict landscape to measure vertical deformation of the eastern Tibetan Plateau. *Journal of Geophysical Research, Earth Surface*, **111**, F03002, doi:10.1029/2005JF000294.

CLARK, M.K., MAHEO G., SALEEBY, J., & FARLEY, K.A. 2006b. The non-equilibrium landscape of the southern Sierra Nevada, California. GSA Today, 15, doi: 10:1130/1052-5173(2005)015<4:TNELOT>2.0.CO;2

CLARK, M. K., FARLEY, K. A., ZHENG, D. W., WANG, Z. C., & A. R. DUVALL A.R. 2010. Early Cenozoic faulting of the northern Tibetan Plateau margin from apatite (U-Th)/He ages. *Earth and Planetary Science Letters*, **296**, 78–88.

COWGILL, E., YIN AN, & HARRISON T.M. 2003. Reconstruction of the Altyn Tagh fault based on U-Pb geochronology: Role of back thrusts, mantle sutures, and heterogeneous crustal strength in forming the Tibetan Plateau. *Journal of Geophysical Research*, **108**, B7-2346, doi:10.1029/2002JB002080.

COWGILL, E., YIN AN, ARROWSMITH, J.R., WANG XIAO FENG, & ZHANG SHUANHONG. 2004a. The Akato Tagh bend along the Altyn Tagh fault, northwest Tibet 1: Smoothing by vertical-axis rotation and the effect of topographic stresses on bend-flanking faults. *Geological Society of America Bulletin*, **116**, 1423-1442, doi:10.1130/B25359.1.

COWGILL, E., ARROWSMITH, J.R., YIN AN, WANG XIAO FENG, & CHEN ZHENGLE. 2004b. The Akato Tagh bend along the Altyn Tagh fault, northwest Tibet 2: Active deformation and the importance of transpression ans strain hardening within the Altyn Tagh system. *Geological Society of America Bulletin*, **116**, 1443-1464, doi.10.1130/B25360.1.

CRADDOCK, W.H., KIRBY, E., ZHANG HUIPING, CLARK, M.K., CHAMPAGNAC, J-D., & YUAN DAOYANG. 2014. Rates and style of Cenozoic deformation around the Gonghe Basin, northeastern Tibetan Plateau. *Geosphere*, **10**, 1255-1282, doi:10.1130/GES01024.1.

DARBY, B.J., RITTS, B.D., YUE, Y., & MENG, Q. 2005. Did the Altyn Tagh fault extend beyond the Tibetan Plateau? *Earth and Planetary Science Letters*, **240**, 425-435.

DEWEY, J.F., & BIRD, J.M. 1970. Mountain belts and the new global tectonics. *Journal of Geophysical Research*, **75**, 2625–2647.

DUVALL, A. R., CLARK, M. K., VAN DER PLUIJM, B. A. & LI, C. 2011. Direct dating of Eocene reverse faulting in northeastern Tibet using Ar-dating of fault clays and low-temperature thermochronometry, *Earth and Planetary Science Letters*, **304**, 520–526.

DUVALL, A.R., CLARK, M.K., KIRBY, E., FARLEY, K.A., CRADDOCK, W.H., LI CHUANYOU, & YUAN DAO-YANG. 2013. Low-temperature thermochronometry along the Kunlun and Haiyuan Faults, NE Tibetan Plateau: Evidence for kinematic change during late-stage orogenesis. *Tectonics*, **32**, 1190-1211, doi:10.1002/tect.20072.

EHLERS, T.A., & FARLEY, K.A. 2003. Apatite (U-Th)/He thermochronology: methods and applications to problems in tectonic and surface processes. *Earth and Planetary Science Letters*, **20**6, 1-14.

ENGLAND, P., & HOUSEMAN, G. 1985. Role of lithospheric strength heterogeneities in the tectonics of Tibet and neighbouring regions. *Nature*, **315**, 297-301.

FENG YUNLEI, YUAN WANMING, TIAN YUNTAO, FENG, XING, HAO NANA, ZHANG LITING, LI YAHAO, LIU QINGSONG, WANG XIAOLONG, SHI ZHEN, ZHU XIAOYONG, WANG KE, & ZHANG AIKUI. 2017. Preservation and exhumation history of the Harizha-Halongxiuma mining area in the East Kunlun Range, Northeastern Tibetan Plateau, China. *Ore Geology Reviews*, **90**, 1018-1031.

FU BIHONG & AWATA Y. 2007. Displacement and timing of left-lateral faulting in the Kunlun Fault Zone, northern Tibet, inferred from geologic and geomorphic features. *Journal of Asian Earth Sciences*, **29**, 253-265.

GALLAGHER, K. 1995. Evolving temperature histories from apatite fission-track data. *Earth and Planetary Science Letters*, **136**, 421-435.

GAN, W., ZHANG, P., SHEN, Z.-K., NIU, Z., WANG, M., WAN, Y., ZHOU, D., & CHENG, J. 2007. Present-day crustal motion within the Tibetan Plateau inferred from GPS measurements, *Journal of Geophysical Research*, **112**, B08416, doi:10.1029/2005JB004120.

GEHRELS, G. E., YIN, A., & WANG, X.F. 2003. Magmatic history of the northeastern Tibetan Plateau. *Journal of Geophysical Research*, **108**, doi: 10.1029:2002JB001876.

GEORGE, A.D., MARSHALLSEA, S.J., WYRWOLL, K.H., JIE, C., & YANCHOU L. 2001. Miocene cooling in the northern Qilian Shan, northeastern margin of the Tibetan plateau, revealed by apatite fission-track and vitrinite reflectance analysis. *Geology*, **29**, 939-942.

GOLDRICK, G, & BISHOP, P. 2007. Regional analysis of bedrock stream long profiles: evaluation of Hack's SL form, and formulation and assessment of an alternative (the DS form). *Earth Surface Processes and Landforms*, **32**, 649-671.

GREEN, P.F., DUDDY, I.R., LASLETT, G.M., HEGARTY, K.A., GLEADOW, A.J.W., & LOVERING, J.F. 1989. Thermal annealing of fission tracks in apatite 4. Quantitative modelling techniques and extension to geological timescales. *Chemical Geology*, **79**, 155-182.

GROVES, K., SAVILLE, CH., HURST, M.D., JONES, S.J., SONG SHUGUANG, & ALLEN, M.B. 2020. Geomorphic expressions of collisional tectonics in the Qilian Shan, north eastern Tibetan Plateau. *Tectonophysics*, **788**, 228503.

GUO, Z., ZHANG, Z., & WANG, J. 1998. Formation and evolution of the Xorkol Basin and its relation to the Altyn Tagh fault. *Geological Journal of China Universities*, **4**, 59–63.

HACKER, B.R., GNOS, E., RATSCHBACHER, L., GROVE, M., MCWILLIAMS, M., SOBOLEV, S.V., WAN, J., & ZHENHAN, W. 2000. Hot and dry deep crustal xenoliths from Tibet. *Science*, **287**, 2463-2466.

HE PENGJU, SONG CHUNHUI, WANG YADONG, CHEN LIHAO, CHANG PENGFEI, WANG QIANGQIANG, & REN BO. 2017. Cenozoic exhumation in the Qilian Shan, northeastern Tibetan Plateau: Evidence from detrital fission track thermochronology in the Jiuquan Basin. *Journal of Geophysical Research: Solid Earth*, **122**, 6910–6927, doi:10.1002/2017JB014216.

HEERMANCE, R., PULLEN, A., KAPP, P., GARZIONE, C., BOGUE, S., DING, L., & SONG, P. 2013. Climatic and tectonic controls on sedimentation and erosion during the Pliocene–Quaternary in the Qaidam Basin (China). *Geological Society of America Bulletin*, **125**, 833-856.

HONG YAN, NIX, H.A., HUTCHINSON, M.F., & BOOTH, T.H. 2005. Spatial interpolation of monthly mean climate data for China. *International Journal of Climatology*, **25**, 1369-1379.

HORN, B.K.P. 1981. Hill shading and the reflectance map. *Proceedings of the IEEE*, **69**, 14-47.

HUANG, X., GAO, R., LI, W., & XIONG, X. 2021. Seismic reflection evidence of crustal duplexing and lithospheric underthrusting beneath the western Qilian Mountains, northeastern margin of the Tibetan Plateau. *Science China, Earth Sciences*, **64**, 96-109.

HURFORD, A.J., & GREEN, P.F. 1983. The zeta age calibration of fission-track dating. *Chemical Geology*, **1**, 285-317.

JI, J., ZHANG, K., CLIFT, P.D., ZHUANG, G., SONG, B., KE, X., & XU, Y. 2017. High-resolution magnetostratigraphic study of the Paleogene-Neogene strata in the Northern Qaidam Basin: Implications for the growth of the Northeastern Tibetan Plateau. *Gondwana Research*, **46**, 141-155.

JIANG XIAODIAN, JIN YU & MCNUTT, M.K. 2004. Lithospheric deformation beneath the Altyn Tagh and West Kunlun faults from recent gravity surveys. *Journal of Geophysical Research*, **109**, B05406, doi:10.1029/2003JB002444.

JOLIVET, M. 2017. Mesozoic tectonic and topographic evolution of Central Asia and Tibet: a preliminary synthesis. *Geological Society of London Special Publication*, **427**, http://doi.org/10.1144/SP427.2

JOLIVET, M., ROGER, F., ARNAUD, N., BRUNEL, M., TAPPONNIER, P., & SEWARD, D. 1999. Histoire de l'exhumation de l'Altun Shan : indications sur l'âge de la subduction du bloc du Tarim sous le système de l'Altyn Tagh (Nord Tibet). *Comptes Rendus de l'Académie des Sciences, Paris*, **329**, 749-755.

JOLIVET, M., BRUNEL, M., SEWARD, D., XU, ZH., YANG, J., ROGER, F., TAPPONNIER, P., MALAVIEILLE, J., ARNAUD, N., & WU, C. 2001. Mesozoic and Cenozoic tectonics of the northern edge of the Tibetan plateau: fission-track constraints. *Tectonophysics*, **343**, 111-134.

JOLIVET, M., BRUNEL, M., SEWARD, D., XU, Z., YANG, J., MALAVIEILLE, J., ROGER, F., LEYRELOUP, A., ARNAUD, N., & WU, C. 2003. Neogene extension and volcanism in the Kunlun Fault Zone, northern Tibet: New constraints on the age of the Kunlun Fault, *Tectonics*, **22**, 1052, doi:10.1029/2002TC001428.

JOLIVET, M., RITZ, J-F., VASSALLO, R., LARROQUE, Ch., BRAUCHER, R., TODBILEG, M., CHAUVET, A., SUE, Ch., ARNAUD, N., DE VICENTE, R., ARZHANNIKOVA, A., &

ARZHANNIKOV, S. 2007. The Mongolian summits : An uplifted, flat, old but still preserved erosion surface. *Geology*, **35**, 871-874.

JOLIVET, M., ROGER, F., XU, Z.Q., PAQUETTE, J.-L., & CAO, H. 2015. Mesozoic – Cenozoic evolution of the Danba dome (Songpan-Garzê, East Tibet) as inferred from LA-ICP-MS U-Pb and fission-track data. *Journal of Asian Earth Sciences*, **102**, 180-204.

KANG GUO FA, GAO GUO MING, BAI CHUN HUA, SHAO DAN, & FENG LI LI. 2012. Characteristics of the crustal magnetic anomaly and regional tectonics in the Qinghai-Tibet Plateau and the adjacent areas. *Science in China – Earth Sciences*, **55**, 1028-1036.

KARPLUS, M.S., ZHAO, W., KLEMPERER, S.L., WU, Z., MECHIE, J., SHI, D., BROWN, L.D., & CHEN C. 2011. Injection of Tibetan crust beneath the south Qaidam Basin: Evidence from INDEPTH IV wide-angle seismic data. *Journal of Geophysical Research*, **116**, B07301, doi:10.1029/2010JB007911.

KARPLUS, M.S., KLEMPERER, S.L., ZHAO WENJIN, KIND, R., WU ZHENHAN, MECHIE, J., SHI DANIAN, BROWN, L.D., CHEN CHEN, SU HEPING, XUE GUANGXI, SANDVOL, E., NI, J., TILMANN, F.J., & CHEN YONGSHUN J. 2019. Receiver-function imaging of the lithosphere at the Lunlun-Qaidam boundary, Northeast Tibet. *Tectonophysics*, **759**, 30-43.

KIDD, W.S.F., & MOLNAR, P. 1988. Quaternary and active faulting observed on the 1985 Academia Sinica – Royal Society Geotraverse of Tibet. *Philosophical Translation of the Royal Society of London*, **A 327**, 337-363.

KOOI, H., & BEAUMONT, C. 1996. Large-scale geomorphology: classical concepts reconciled and integrated with contemporary ideas via a surface processes model. *Journal of Geophysical Research*, **101**, 3361-3386.

KONSTANTINOVSKAIA, E.A., BRUNEL, M., & MALAVIEILLE, J. 2003. Discovery of the Paleo Thethys residual peridotites along the Anyemaqen-Kunlun suture zone (North Tibet). Comptes Rendus Géoscience, 335, 709-719.

LASLETT, G.M., GREEN, P.F., DUDDY, I.R., & GLEADOW, A.J.W. 1987 Thermal annealing of fission tracks in apatite, 2. A quantitative analysis. *Chemical Geology*, **65**, 1-13.

LASSERRE, C., MOREL, P.H., GAUDEMER, Y., TAPPONNIER, P., RYERSON ,F.J., KING, G.C.P., MÉTIVIER, F., KASSER, M., KASHGARIAN, M., BAICHI, L., TAIYA, L., & DAOYANG, Y. 1999. Postglacial left slip rate and past occurrence of M ≥ 8 earthquakes on the western Haiyuan fault, Gansu, China. *Journal of Geophysical Research*, **104**, 17633-17651.

LEASE, R.O., BURBANK, D.W., CLARK, M.K., FARLEY, K.A., ZHENG DEWEN, & ZHANG HUIPING. 2011. Middle Miocene reorganization of deformation along the northeastern Tibetan Plateau. *Geology*, **39**, 359-362.

LEOPOLD, L. B., & MADDOCK, T. 1953. The hydraulic geometry of stream channels and some physiographic implications. *Professional Paper*, Washington.

LI BING, CHEN XUANHUA, ZUZA, A.V., HU DAOGONG, DING WEICUI, HUANG PENGHUI, & XU SHENGLIN. 2019. Cenozoic cooling history of the North Qilian Shan, northern Tibetan Plateau, and the initiation of the Haiyuan fault: Constraints from apatite- and zircon-fission track thermochronology. *Tectonophysics*, **751**, 109-124.

LI BING, ZUZA, A.V., CHEN XUANHUA, SHAO ZHAOGANG, QI BANGSHEN, WANG ZENG-ZHEN, LEVY, D.A., & XIONG XIAOSONG. 2020. Cenozoic multi-phase deformation in the Qilian Shan and out-of-sequence development of the northern Tibetan Plateau. Tectonophysics, 782, 228423.

LI BING, ZUZA, A.V., CHEN XUANHUA, WANG ZENG-ZHEN, SHAO ZHAOGANG, LEVY, D.A., WU CHEN, XU SHENGLIN, & SUN YUJUN. 2021. Pre-cenozoic evolution of the northern Qilian Orogen from zircon geochronology: Framework for early growth of the northern Tibetan Plateau. *Palaeogeography, Palaeoclimatology, Palaeoecology*, **562**, 110091, https://doi.org/10.1016/j.palaeo.2020.110091.

LI CHAOPENG, ZHENG DEWEN, ZHOU RENJIE, YU JINGXING, WANG YIZHOU, PANG JIANZHANG, WANG YIN, HAO YUQI & LI YOUJUAN. 2021. Late Oligocene tectonic

uplift of the East Kunlun Shan: Expansion of the northeastern Tibetan Plateau. *Geophysical Research Letters*, **48**, e2020GL091281. https://doi. org/10.1029/2020GL091281.

LI, J., YUE, L., ROBERTS, A., HIRT, A.M., PAN, F., GUO, L., XU, Y., XI, R., GUO, L., QIANG, X. 2018. Global cooling and enhanced Eocene Asian mid-latitude interior aridity. *Nature Communications*, **9**, 3026.

LI LUN, ZHANG XUEZHEN, LIAO JIE, LIANG YANLING & DONG SHIXIAN. 2021. Geophysical constraints on the nature of lithopshere in central and eastern Tibetan plateau. *Tectonophysics*, **804**, 228722, https://doi.org/10.1016/j.tecto.2021.228722.

LI MENG, TANG LIANGJIE, & YUAN WANMING. 2015. Middle Miocene-Pliocene activities of the North Altyn fault system : Evidence from apatite fission track data. *Arabian Journal of Geosciences*, **8**, 9043-9054.

LIN, X., JOLIVET, M., LIU-ZENG, J., CHENG, F., TIAN, Y., & LI, C. 2021. Mesozoic-Cenozoic cooling history of the eastern Qinghai Nan Shan (NW China): apatite low-temperature thermochronology constraints from the deep canyon of the Yellow River. *Palaeogeography, Palaeoclimatology, Palaeoecology*, **572**, 110416. https://doi.org/10.1016/j.palaeo.2021.110416.

LIU DONGLIANG, LI HAIBING, SUN ZHIMING, PAN JIAWEI, WANG MENG, WANG HUAN, & CHEVALIER, M-L. 2017. AFT dating constrains the Cenozoic uplift of the Qimen Tagh Mountains, Northeast Tibetan Plateau, comparison with LA-ICPMS Zircon U–Pb ages. *Gondwana Research*, **41**, 438-450.

LIU DONGLIANG, LI HAIBING, CHEVALIER, M-L., SUN ZHIMING, PEI JUNLING, PAN JIAWEI, GE CHENGLONG, WANG PING, WANG HUAN, & WU CHAN. 2021. Activity of the Baiganhu fault of the Altyn Tagh fault system, northern Tibetan Plateau: Insights from zircon and apatite fission track analyses. *Palaeogeography, Palaeoclimatology, Palaeoecology*, **570**, 110356, https://doi.org/10.1016/j.palaeo.2021.110356

LIU, Z.Q. (Ed). 1988. Geological map of Qinghai-Xizang (Tibet) plateau and adjacent areas, scale 1 :1,500,000. Geol. Publ., Beijing, 91 pp.

LIU-ZENG, J., TAPPONNIER, P., GAUDEMER, Y., & DING, L. 2008. Quantifying landscape differences across the Tibetan plateau: Implications for topographic relief evolution. *Journal of Geophysical Research*, **113**, F04018, doi:10.1029/2007JF000897.

LU HAIJIAN, WANG ERCHIE, SHI XUHUA, & MENG KAI. 2012. Cenozoic tectonic evolution of the Elashan range and its surroundings, northern Tibetan Plateau as constrained by paleomagnetism and apatite fission track analyses. *Tectonophysics*, **580**, 150-161.

MATTE, P., TAPPONNIER, P., ARNAUD, N., BOURJOT, L., AVOUAC, J.P., VIDAL, P., LIU, Q., PAN, Y., & WANG, Y. 1996. Tectonics of Western Tibet, between the Tarim and the Indus. *Earth and Planetary Science Letters*, **142**, 311-330.

MATTINSON, C.G., MENOLD, C.A., ZHANG, J.X., & BIRD, D.K. 2007. High- and ultrahigh-pressure metamorphism in the North Qaidam and South Altyn terranes, Western China. *International Geology Reviews*, **49**, 969-995.

MENG KAI, WANG ERCHIE, CHU, J.J., SU ZHE, & FAN CHUN. 2020. Late Cenozoic river system reorganization and its originwithin the Qilian Shan, NE Tibet. *Journal of Structural Geology*, **138**, 104128, https://doi.org/10.1016/j.jsg.2020.104128.

MENG, L., & CUI, J. 1997. Study on the Gravity field and Deep-Seated Crustal Structure at the North Margin of the Qinghai-Tibet Plateau. *Continental Dynamics*, **2**, 29-38.

MENOLD, C.A., MANNING, C.E., YIN, A., TROPPER, P., CHEN, X-H., & WANG, X-F. 2009. Metamorphic evolution, mineral chemistry and thermobarometry of orthogneiss hosting ultrahigh-pressure eclogites in the North Qaidam metamorphic belt, Western China. *Journal of Asian Earth Sciences*, **35**, 273-284.

MEYER, B., TAPPONNIER, P., BOURJOT, L., MÉTIVIER, F., GAUDEMER, Y., PELTZER, G., SHUNMIN, G., & ZHITAI, C. 1998. Crustal thickening in Gansu-Qinghai, lithospheric mantle

subduction, and oblique, strike-slip controlled growth of the Tibet plateau. *Geophysical Journal Internationa*l, **135**, 1-47.

MEYER, B., SALTUS, R., & CHULLIAT, A. 2017. EMAGG2v3: Earth Magnetic Anomaly Grid (2-arc-minute resolution). Version 3. NOAA National Centers for Environmental Information. https://doi.org/10.7289/V5H70CVX. Accessed 06-30-2021.

MINISTRY OF GEOLOGY AND NATURAL RESSOURCES. 1980. Geological map of the Qinghai-Xizang (Tibet) Plateau (1 :1.5 Million scale). *Ministry of Geology and Natural Resources*, Beijing.

MOCK, C., ARNAUD, N.O., & CANTAGREL, J.M.. 1999. An early unroofing in northeastern Tibet ? Constraints from 40Ar/39Ar thermochronology on granitoïds from the eastern Kunlun range (Qianghai, NW China). *Earth and Planetary Science Letters*, **17**1, 107-122.

MOLNAR, P., & TAPPONNIER, P. 1975. Cenozoic Tectonics of Asia : Effects of a continental Collision., *Science*, **189**, 419-426.

MORIN, J., JOLIVET, M., BARRIER, L., LABORDE, A., HAIBING LI., & DAUTEUIL O. 2019. Planation surfaces of the Tian Shan range (Central Asia): Insight on several 100 Myrs of topographic evolution. *Journal of Asian Earth Sciences*, **177**, 52-65.

PELTZER, G., TAPPONNIER, P., & ARMIJO, R. 1989 Magnitude of late Quaternary left-lateral displacements along the northern edge of Tibet. *Science*, **246**, 1285-1289.

PEYRON, J.T., & ROYDEN, L. 2013. An integral approach to bedrock river profile analysis. *Earth Surface Processes and Landforms*, **38**, 570-576.

QI BANGSHEN, HU DAOGONG, YANG XIAOXIAO, ZHANG YAOLING, TAN CHENGXUAN, ZHANG PENG, & FENG CHENGJUN. 2016. Appatite fission track evidence for the Cretaceous – Cenozoic cooling history of the Qilian Shan (NW China) and for stepwise northeastward growth of the northeastern Tibetan Plateau since early Eocene. *Journal of Asian Earth Sciences*, **124**, 28-41.

RITTS, B.D., & BIFFI, U. 2000. Magnitude of post-Middle Jurassic (Bajocian) displacement on the central Altyn Tagh fault system, northwest China. *Geological Society of America Bulletin*, **112**, 61-74.

RITTS, B. D., YUE, Y., & GRAHAM, S. A. 2004. Oligocene-Miocene tectonics and sedimentation along the Altyn Tagh fault, northern Tibetan Plateau: Analysis of the Xorkol, Subei, and Aksay basins. *Journal of Geology*, **112**, 207–230.

ROBL, J., HERGARTEN, S., & PRASICEK, G. 2017. The topographic state of fluvially conditioned mountain ranges. *Earth-Science Reviews*, **168**, 190-217.

ROGER, F., JOLIVET, M., CATTIN, R., & MALAVIEILLE, J. 2011. Mesozoic-Cenozoic tectonothermal evolution of the eastern part of the Tibetan plateau (Songpan-Garzê, Longmen Shan area): insights from thermochronological data and simple thermal modeling. *Geological Society of London Special Publication*, **353**, 9-25. doi: 10.1144/SP353.2

SEARLE, M., ELLIOTT, J., PHILLIPS, R., & CHUNG, S.L. 2011. Crustal-lithopsheric structure and continental extrusion of Tibet. *Journal of the Geological Society, London*, **168**, 633-672.

SMITH, W.H.F., & WESSEL, P. 1990. Gridding with continuous curvature splines in tension. *Geophysics*, **55**, 293–305.

SOBEL, E.R., & ARNAUD, N. 1999. A possible middle Paleozoic suture in the Altyn Tagh, NW China. *Tectonics*, **18**, 64-74.

SOBEL, E.R., ARNAUD, N., JOLIVET, M., RITTS, B.D., & BRUNEL, M. 2001. Jurassic to Cenozoic exhumation history of the Altyn Tagh range, NW China, constrained by $^{40}Ar/^{39}Ar$ and apatite fission track thermochronology. In Hendrix, M.S., and Davis, G.A. eds., *Paleozoic and Mesozoic tectonic evolution of central Asia: From continental assembly to intracontinental deformation*; Boulder, Colorado, *Geological Society of America Memoir*, **194**, 247-267.

SONG, S.-G., YANG, J.-S., LIOU, J.-G., WU, C.-L., SHI, R.-D., & XU, Z.-Q. 2003. Petrology, Geo-chemistry and isotopic ages of eclogites in the Dulan UHPM terrane, the North Qaidam, NWChina. *Lithos*, **70**, 195–211.

SONG, S.-G., NIU, Y.-L., ZHANG, L.-F., WEI, C.-J., LIOU, J.-G., & SU, L. 2009. Tectonic evolution of Early Paleozoic HP metamorphic rocks in the North Qilian Mountains, NW China: a perspective. *Journal of Asian Earth Science*, **35**, 285–297.

STAISCH, L.M., NIEMI, N.A., CLARK, M.K., & CHANG HONG. 2020. The Cenozoic evolution of crustal shortening and left-lateral shear in the Central East Kunlun Shan: Implications for the uplift history of the Tibetan Plateau. *Tectonics*, **39**, e2020TC006065, https://doi.org/10.1029/2020TC006065.

TAPPONNIER, P., PELTZER, P., & ARMIJO, R. 1986. On the mechanics of the collision between India and Asia. *Geological Society of London Special Publication*, **19**, 113-157.

TAPPONNIER, P., MEYER, B., AVOUAC, J.P., PELTZER, G., GAUDEMER, Y., GUO SHUNMIN, XIANG HONGFA, YIN KELUN, CHEN ZHITAI, CAI SHUAHUA & DAI HUAGANG. 1990. Active thrusting and folding in the Qilian Shan, and decoupling between upper crust and mantle in northeastern Tibet. *Earth and Planetary Science Letters*, **97**, 382-403.

TAPPONNIER, P., XU, Z., ROGER, F., MEYER, B., ARNAUD, N., WITTLINGER, G., & YANG, J. 2001. Oblique Stepwise Rise and Growth of the Tibet Plateau. *Science*, **294**, 1671-1677.

TAYLOR, M., & YIN, A. 2009. Active structures of the Himalayan-Tibetan orogen and their relationships to earthquake distribution, contemporary strain field, and Cenozoic volcanism. *Geosphere*, **5**, 199-214.

TIAN PENGFEI, YUAN WANMING, YANG XIAOYONG, FENG ZIRUI, CHEN XUE, & YUAN ERJUN. 2020. Multi-stage tectonic events of the Eastern Kunlun Mountains, Northern Tibetan Plateau constrained by fission track thermochronology. *Journal of Asian Earth Sciences*, **198**, 104428, https://doi.org/10.1016/j.jseaes.2020.104428.

TURCOTTE, D.L., & SCHUBERT, G. 1982. *Geodynamics: applications of continuum physics to geological problem*s. John Wiley & Sons.

TURNER, S., ARNAUD, N., LIU, J., ROGERS, N., HAWKESWORTH, C., HARRIS, N., KELLEY, S., VAN CALSTEREN, P., & DENG, W. 1996. Post-collision, Shoshonitic Volcanism on the Tibetan Plateau : Implications for Convective Thinning of the Lithosphere and the Source of Ocean Island Basalts. *Journal of Petrology*, **37**, 45-71.

VASSALLO, R., JOLIVET, M., RITZ, J-F., BRAUCHER, R., LARROQUE, Ch., SUE, Ch., TODBILEG, M., & JAVKHLANBOLD, D. 2007. Uplift age and rates of the Gurvan Bogd system (Gobi-Altay) by apatite fission track analysis. *Earth and Planetary Science Letters*, **259**, 333_346.

VINCENT, S.J., & ALLEN, M.B. 1999. Evolution of the Minle and Chaoshui Basins, China : Implications for Mesozoic strike-slip basin formation in Central Asia. *Geological Society of America Bulletin*, **111**, 725-742.

WANG AN, WANG GUOCAN, XIE DEFAN, & LIU DEMIN. 2006. Fission track geochronology of Xiaonanchuan pluton and the morphotectonic evolution of Eastern Kunlun since Late Miocene. *Journal of the China University of Geosciences*, **17**, 302-309.

WANG CHAO, LIU LIANG, YANG WEN-QIANG, ZHU XIAO-HUI, CAO YU-TING, KANG LEI, CHEN SHE-FA, LI RONG-SHE, & HE SHI-PING. 2013. Provenance and ages of the Altyn complex in Altyn Tagh: Implications for the early Neoproterozoic evolution of northwestern China. *Precambrian Research*, **230**, 193-208.

WANG ERCHIE, XU FENG-YIN, ZHOU JIAN-XUN, WAN JINGLIN & BURCHFIELD, B.C. 2006. Eastward migration of the Qaidam basin and its implications for Cenozoic evolution of the Altyn Tagh fault and associated river systems. *Geological Society of America Bulletin*, **118**, 349-365, doi:10.1130/B25778.1.

WANG ERCHIE, XU FENG-YIN, ZHOU JIAN-XUN, WANG SHIFENG, FAN CHUNG & WANG GANG. 2008. Vertical-axis bending of the Altyn Tagh belt along the Altyn Tagh fault: Evidence from late Cenozoic deformation within and around the Xorkol Basin. *in* Burchfiel,

B.C., and Wang, E., eds., *Investigations into the Tectonics of the Tibetan Plateau. Geological Society of America Special Paper*, **444**, 1–20, doi: 10.1130/2008.2444(07) .

WANG FEI, LO CHING-HUA, LI QI, YEH MENG-WAN, WAN JINGLIN, ZHENG DEWEN, & WANG ERQI. 2004. Onset timing of significant unroofing around Qaidam basin, northern Tibet, China: constraints from $^{40}Ar/^{39}Ar$ and FT thermochronology on granitoids. *Journal of Asian Earth Sciences*, **24**, 59-69.

WANG LIN, CHENG FENG, ZUZA, A.V., JOLIVET, M., LIU YIDUO, GUO ZHAOJIE, LI XIANGZHOU, & ZHANG CHANGHAO. 2021. Diachronous growth of the northern Tibetan plateau derived from flexural modeling. *Geophysical Research Letters*, **48**, e2020GL092346. https://doi-org.insu.bib.cnrs.fr/10.1029/2020GL092346

WANG MIN, & SHEN ZHENG-KANG. 2019. Present-Day crustal deformation of continental China derived from GPS and its tectonic implications. *Journal of Geophysical Research – Solid Earth*, **125**, e2019JB018774. https://doi.org/ 10.1029/2019JB018774.

WANG WEITAO, ZHENG WENJUN, ZHANG PEIZHEN., LI QIANG, KIRBY, E., YUAN DAOYANG, ZHENG DEWEN, LIU CAICAI, WANG ZHICAI, ZHANG HUIPING, & PANG JIANZHANG. 2017. Expansion of the Tibetan Plateau during the Neogene. *Nature Communications*, **8**, 15887. https://doi.org/10.1038/ncomms15887.

WANG XIUXI, SONG CHUNHUI, ZATTIN, M., HE PENGJU, SONG AI, LI JIJUN, & WANG QIANGQIANG. 2016. Cenozoic pulsed deformation history of northeastern Tibetan Plateau reconstructed from fission-track thermochronology. *Tectonophysics*, **672-673**, 212-227.

WANG YADONG, ZHENG JIANJING, & ZHENG YOUWEI. 2018. Mesozoic-Cenozoic exhumation history of the Qimen Tagh Range, northeastern margins of the Tibetan Plateau: Evidence from apatite fission track analysis. *Gondwana Research*, **58**, 16-26.

WANG YE, CHEN XUANHUA, ZHANG YAOTAO, YIN ZHENG, ZUZA, A.V., YIN AN, WANG YONGCHAO, DING WEICUI, XU SHENGLIN, ZHANG YIPING, LI BING, & SHAO ZHAOGANG. 2021. Superposition of Cretaceous and Cenozoic deformation in northern Tibet:

A far-field response to the tectonic evolution of the Tethyan orogenic system. *Geological Society of America Bulletin*, https://doi.org/10.1130/B35944.1

WELLER, O.M., ST-ONGE, M.R., WATERS, D.J., RAYNER, N., SEARLE, M.P., CHUNG, S.-L., PALIN, R.M., LEE, Y.-H., & XU, X. 2013. Quantifying Barrovian metamorphism in the Danba Structural Culmination of eastern Tibet. *Journal of Metamorphic Geology*, doi:10.1111/jmg.12050.

WESSEL, P., & SMITH, W.H.F. 1991. Free software helps map and display data. *EOS Transactions American Geophysical Union,* **72**, 441, 445-446.

WHICKERT A.D., & SCHILGEN T.F. 2019. Long-profile evolution of transport-limited gravel-bed rivers. *Earth Surface Dynamics*, **7**, 17-43.

WHIPPLE, K.X., & TUCKER, G.E. 2002. Implications of sediment-flux-dependent river incision models for landscape evolution. Journal of Geophysical Research, Solid Earth, 107, 2039, https://doi.org/10.1029/2000JB000044

WHIPPLE, K.X. 2004. Bedrock rivers and the geomorphology of active orogens. *Annual Review of Earth and Planetary Sciences*, **32(1)**, 151–185.

WILLETT, S.D., & BRANDON, M.T., 2002. On Steady states in mountain belts. *Geology*, **30**, 175-178.

WITTLINGER, G., TAPPONNIER, P., POUPINET, G., MEI, J., DANIAN, S., HERQUEL, G.,& MASSON, F. 1998. Tomogaphic evidence for localized lithospheric shear along the Altyn Tagh fault. *Science*, **282**, 74-76.

WU CHEN, YIN AN, ZUZA, A.V., ZHANG JINYU, LIU WENCAN, & DING LIN. 2016. Pre-Cenozoic geologic history of the central and northern Tibetan Plateau and the role of Wilson cycles in constructing the Tethyan orogenic system. *Lithosphere*, **8**, 254–292. https://doi.org/ 10.1130/L494.1.

WU, C., ZUZA, A.V., CHEN, X.H., DING, L., LEVY, D.A., LIU, C.F., LIU, W.C., JIANG, T., & STOCKLI, D.F. 2019. Tectonics of the Eastern Kunlun Range: Cenozoic reactivation of a Paleozoic–early Mesozoic orogen. *Tectonics*, **38**, 1609–1650.

WU CHEN, LI JIE, ZUZA, A.V., LIU CHANGFENG, LIU WENCAN, CHEN XUANHUA, JIANG TIAN & LI BING. 2020. Cenozoic cooling history and fluvial terrace development of the western domain of the Eastern Kunlun Range, northern Tibet. *Palaeogeography, Palaeoclimatology, Palaeoecology*, **560**, 109971.

WU CHEN, ZUZA, A.V., LI JIE, HAPROFF, P.J., YIN AN, CHEN XUANHUA, DING LIN, & LI BINg. 2021. Late Mesozoic-Cenozoic cooling history of the northeastern Tibetan Plateau and its foreland derived from low-temperature thermochronology. *Geological Society of America Bulletin*, https://doi.org/10.1130/B35879.1.

WU, G., GAO, R., CUI, Z., & WU, X. 1996. Preliminary Study on Geophysical Data in Qilian Mountains. *Continental Dynamics*, **1**, 10-19.

YANG, J., XU, ZH., SONG, S., WU, C., SHI, R., ZHANG, J., WAN, Y., LI, H., JIN, X., & JOLIVET M. 2000. Discovery of eclogite in Dulan, Qinghai Province and its significance for studying the HP-UHP metamorphic belt along the central orogenic belt of China. *Acta Geologica Sinica*, **74**, 154 -168.

YIN AN, & HARRISON, T.M. 2000. Geologic evolution of the Himalayan-Tibetan orogen. *Annual Review of Earth Planetary Science Letters*, **28**, 211-280.

YIN AN, RUMELHART, P.E., BUTLER, R., COWGILL, E., HARRISON, T.M., FOSTER, D.A., INGERSOLL, R.V., ZHANG QING, ZHOU XIAN-QIANG, WANG XIAO-FENG, HANSON, A., & RAZA, A. 2002. Tectonic history of the Altyn Tagh fault system in northern Tibet inferred from Cenozoic sedimentation. G*eological Society of America Bulletin*, **114**, 1257-1295.

YIN AN, DANG YUQI, ZHANG MIN, McRIVETTE, M.W., BURGESS, W.P., & CHEN XUANHUA 2007A. Cenozoic tectonic evolution of Qaidam basin and its surrounding regions

(part 2): Wedge tectonics in southern Qaidam basin and the Eastern Kunlun Range. *in* Sears, J.W., Harms, T.A., and Evenchick, C.A., eds., Whence the Mountains? Inquiries into the Evolution of Orogenic Systems: A Volume in Honor of Raymond A. Price: *Geological Society of America Special Paper*, **433**, 369–390, doi: 10.1130/2007.2433(18).

YIN AN, MANNING, C.E., LOVERA, O., MENOLD, C.A., CHEN XUANHUA, & GEHRELS, G.E. 2007b. Early Paleozoic tectonic and thermomechanical evolution of ultrahigh-pressure (UHP) metamorphic rocks in the Northern Tibetan Plateau, Northwest China. *International Geology Review*, **49**, 681-716.

YIN, A., DANG, Y-Q., ZHANG, M., CHEN, X-H., & MCRIVETTE, M.W. 2008. Cenozoic tectonic evolution of the Qaidam basin and its surrounding regions (Part 3): Structural geology, sedimentation, and regional tectonic reconstruction. *Geological Society of America Bulletin*, **120**, 847-876.

YE ZHUO, GAO RUI, LI QIUSHENG, ZHANG HONGSHUANG, SHEN XUZHANG, LIU XUZHOU, & GONG CHEN. 2015. Seismic evidence for the North China plate underthrusting beneath northeastern Tibet and its implications for plateau growth. *Earth and Planetary Science Letters*, **426**, 109-117. http://dx.doi.org/10.1016/j.epsl.2015.06.024

YU JUNGXING, PANG JIANZHANG, WANG YIZHOU, ZHENG DEWEN, LIU CAICAI, WANG WEITAO, LI YOUJUAN, LI CHAOPENG, & XIAO LIN. **2019**. Mid-Miocene uplift of the northern Qilian Shan as a result of the northward growth of the northern Tibetan Plateau. *Geosphere*, **15**, 423–432, https://doi.org/10.1130/GES01520.1.

YUAN DAO-YANG, CHAMPAGNAC, J-D., GE WEI-PENG, MOLNAR, P., ZHANG PEI-ZHEN, ZHENG WEN-JUN, ZHANG HUI-PING, & LIU XING-WANG. 2011. Late Quaternary right-lateral slip rates of faults adjacent to the lake Qinghai, northeastern margin of the Tibetan Plateau. *Geological Society of America Bulletin*, **123**, 2016-2030

YUAN DAO-YANG, GE WEI-PENG, CHEN ZHEN-WEI, LI CHUAN-YOU, WANG ZHI-CAI, ZHANG HUI-PING, ZHANG PEI-ZHEN, ZHENG DE-WEN, ZHENG WEN-JUN,

CRADDOCK, W.H., DAYEM, K.E., DUVALL, A.R., HOUGH, B.G., LEASE, R.O., CHAMPAGNAC, J-D., BURBANK, D.W., CLARK, M.K., FARLEY, K.A., GARZIONE, C.N., KIRBY, E., MOLNAR, P., & ROE, G.H. 2013. The growth of northeastern Tibet and its relevance to large-scale continental geodynamics: A review of recent studies. *Tectonics*, **32**, 1358-1370.

YUAN WANMING, DONG JINQUAN, WANG SHICHENG, & CARTER, A. 2006. Apatite fission track evidence for neogene uplift in the eastern Kunlun Mountains, northern Qinghai-Tibet Plateau, China. *Journal of Asian Earth Sciences*, **27**, 847-856.

YUE YONGJUN, RITTS, B.D., GRAHAM, S.A., WOODEN, J.L., GEHRELS, G.E., & ZHANG ZHICHENG. 2003. Slowing extrusion tectonics: lowered estimate of post-Early Miocene slip rate for the Altyn Tagh fault. *Earth and Planetary Science Letters*, **217**, 111-122.

ZHANG, J.X., MATTINSON, C.G., YU, S.Y., & LI, Y.S. 2014. Combined rutile-zircon thermometry and U-Pb geochronology: New constraints on Early Paleozoic HP/UHT granulite in the south Altyn Tagh, north Tibet, China. *Lithos*, **200-201**, 241-257.

ZHANG LETIAN, UNSWORTH, M., JIN SHENG, WEI WENHO, YE GAOFENG, JONES, A.G., JING JIANEN, DONG HAO, XIE CHENGLIANG, LE PAPE, F., & VOZAR, J. 2015. Structure of the Central Altyn Tagh Fault revealed by magnetotelluric data: New insights into the strcuture of the northern margin of the India-Asia collision. *Earth and Planetary Science Letters*, **415**, 67-79.

ZHAO JUNGMENG, MOONEY, W.D, ZHANG XIANKANG, LI ZHICHUN, JIN ZHIJUN & OKAYA, N. 2006. Crustal structure across the Altyn Tagh Range at the northern margin of the Tibetan plateau and tectonic implications. *Earth and Planetary Science Letters*, **241**, 804-814.

ZHAO XUDONG, ZHAO JUNFENG, ZENG XU, TIAN JIXIAN, GUO ZEQING, WANG CHAO, WANG DI, & HI CHAO. 2020. Early-Middle Jurassic paleogeography reconstruction in the Western Qaidam Basin: Insights from sedimentology and detrital zircon geochronology.

Marine and Petroleum Geology, **118**, 104445, https://doi.org/10.1016/j.marpetgeo.2020.104445.

ZHENG, D., WANG, W., WAN, J., YUAN, D., LIU, C., ZHENG, W., ZHANG H., PANG J., & ZHANG P. 2017. Progressive northward growth of the northern Qilian Shan-Hexi Corridor (northeastern Tibet) during the Cenozoic. *Lithosphere*, **9**, 408–416. https://doi.org/10.1130/L587.1.

ZENG, W., ZHANG, H.P., ZHANG, P.Z., MOLNAR, P., LIU, X.W. & YUAN, D.Y., 2013a. Late Quaternary slip rates of the thrust faults in western Hexi Corridor (Northern Qilian Shan, China) and their implications for northeastward growth of the Tibetan Plateau. *Geosphere*, **9(2)**, 342-354.

ZUZA, A.V., CHENG, X., & YIN, A. 2016. Testing models of Tibetan Plateau formation with Cenozoic shortening estimates across the Qilian Shan–Nan Shan thrust belt. *Geosphere*, **12**, 501–532. https://doi.org/10.1130/GES01254.1.

ZUZA, A.V., & YIN AN. 2016. Continental deformation accommodated by non-rigid passive bookshelf faulting: An exemple from the Cenozoic tectonic development of northern Tibet. *Tectonophysics*, **677-678**, 227-240.

ZUZA, A.V., WU, C., REITH, R.C., YIN, A., LI, J.H., ZHANG, J.Y., ZHANG, Y.X., WU, L., & LIU, W.C. 2018. Tectonic evolution of the Qilian Shan: an early Paleozoic orogen re- activated in the Cenozoic. *Geological Society of America Bulletin*, **130**, 881–925. https://doi.org/10.1130/B31721.1.

ZUZA, A.V., WU, C., WANG, Z.Z., LEVY, D., LI, B., XIONG, X.S., CHEN, X.H. 2019. Underthrusting and duplexing beneath the northern Tibetan Plateau and the evolu- tion of the Himalayan-Tibetan orogen. *Lithosphere*, **11**, 209–231. https://doi.org/10. 1130/L1042.1.

Figure captions

Figure 1: (**a**) Topography of North Tibet drawn from SRTM-1 digital elevation data showing the main fault systems (compiled mostly from Jolivet et al., 2001 and Taylor and Yin, 2009). The grey arrows represent GPS-measured horizontal displacements (data from Wang and Shen, 2019). The black lines indicate the position of the geological cross-sections presented in Figure 2. (**b**) Slope map (in degrees) of North Tibet calculated using the GMT Software based on SRTM-1 data. The coloured circles represent the apatite fission track data available in the region (see the text for references in each sub-region).

Figure 2: Regional geological cross-sections (see Figure 1 for the position of the sections). (**a**) Across the Altun Shan, showing the major shear zones of the Altyn Tagh and North Altyn Tagh (North ATF) faults that control the vertical, block-like uplift of the Altun Shan range. (**b**) From the eastern part of East Kunlun to North China Block in the southern reach of the Hexi Corridor. Lithospheric subduction in the Kunlun is absent or very limited, while more pronounced in the Qilian Shan. The crustal deformation is largely accommodated through crustal buckling between the Kunlun fault and Haiyuan fault. The latests are major shear zones super-imposed to former suture zones (the Anyemaquen and Central Qilian Shan sutures). The Elashan fault probably corresponds to a Cenozoic structure. The oceanic paleo-slab below the Qilian Shan is inferred from geophysical data (Chen et al., 2019; Li et al., 2020). (**c**) From the Qimen Tagh range to the Yumen Basin. The occurrence of volcanism in the western part of East Kunlun, as well as the geometry of the ranges suggest well developed lithospheric subduction of the Qaidam Block below Tibet. A mid-crustal detachment, possibly developing along the fragile to ductile crust interface propagates the deformation to the NE. The Danghe Nanshan thrust, superposed to the Central Qilian Shan suture zone, limits this propagation and the Central Qilian Shan Block forms a backstop to a second crustal prism developing toward

the North China Block. The oceanic paleo-slab is poorly documented and may represent a continuation, toward the north, of the slab observed further south. See text for a complete discussion of the sections and references.

Figure 3: Topography and fault pattern of the Altun Shan range. (**a**) Landsat / Copernicus image (sourced from Google Earth) of the Altun Shan Range. ATF: Altyn Tagh Fault; NAT-TF: North Altyn Tagh Thrust Fault; Ak.: Akato Tagh; Aka.: Akatengmeng Shan. The white rectangles labelled P1 to P4 correspond to the location of the swath topographic profiles shown on Figure 6. The blue lines labelled R1 to R5 correspond to the river profiles shown on Figure 6. (**b**) Topographic map of the plateau surface west of the Xorkol Basin (drawn from SRTM-1 data). (**c**) Slope map of the same area.

Figure 4: Topography and fault pattern of the East Kunlun Range. (**a**) Landsat / Copernicus image (sourced from Google Earth) of the East Kunlun Range. Caption as on Figure 3. Swath topographic profiles P1 to P5 as well as river profiles R1 to R4 are shown on Figure 7. (**b**) Maxar Technologies / CNES / Airbus image (sourced from Google Earth) of a preserved planation surface in the eastern part of the East Kunlun Range. (**c**) Slope map of the same area obtained from SRTM-1 data.

Figure 5: Topography and fault pattern of the Qilian Shan Range. (**a**) Landsat / Copernicus image (sourced from Google Earth) of the Qilian Shan. Longyang G: Longyang Gorges. Swath topographic profiles P1 to P4 as well as river profiles R1 to R4 are shown on Figure 8. (**b**) Maxar Technologies / CNES / Airbus image (sourced from Google Earth) of a preserved planation surface west of Lake Hala. IC: Ice cap. (**c**) Slope map of the same area obtained from SRTM-1 data. (**d**) Landsat / Copernicus image (sourced from Google Earth) of preserved

planation surfaces (S1 to S8) NW of Lake Qinghai. (**e**) Slope map of the same area obtained from SRTM-1 data.

Figure 6: Conceptual models showing the three modes of crustal deformation: Distributed shortening, block uplift and crustal buckling, as well as the associated topographic and erosion patterns. On the schematic maps (top), the grey dotted lines are iso-altitude lines, the black lines are rivers. On the cross sections (middle), the black arrows indicate uplift, the grey-shaded areas represent the eroded material, the black lines are faults. The erosion versus distance graphs indicate the variation of erosion rates along the topographic transects.

Figure 7: Topographic swath profiles and longitudinal river profiles across the Altun Shan Range obtained from SRTM-1 data. See Figure 3 for location and text for discussion. On profiles Topo 1 and Topo 2, the very low altitude values (reaching 0 m) are linked to gaps in the SRTM data. ATF: Altyn Tagh Fault, Ak. , Aka.: Akato Tagh, Akatengmeng Shan, Jin.: Jinyan Shan K1 and K2: knickpoints. F1, F2 and F3 refer to major faults (see Fig. 3 for location on a map). NAT-FT is the North Altyn Tagh Thrust Fault.

Figure 8: Topographic swath profiles and longitudinal river profiles across the East Kunlun Range obtained from SRTM-1 data. See Figure 4 for location and text for discussion. KF: Kunlun Fault. K1 and K2: knickpoints.

Figure 9: Topographic swath profiles and longitudinal river profiles across the Qilian Shan Range obtained from SRTM-1 data. See Figure 5 for location and text for discussion. K1 to K3: knickpoints.

Figure 10: Schematic 3D structure of the North Tibet crust showing the relation between the main blocks and the surface deformation pattern. The wide dotted line between the Kunlun and Haiyuan faults represents the potential new shear zone accommodating the differential motion between the NW and SE Qaidam – South Qilian Shan blocks. ATF: Altyn Tagh Fault; NCB: North China Block; EF: Elashan Fault; HF: Haiyuan Fault; KF: Kunlun Fault; NATF: North Altyn Tagh Fault; TB: Tarim Block.

Figure 11: EMAG2v3 magnetic anomaly map of North Tibet (Meyer et al., 2017). The near E – W negative anomaly across the Qaidam Basin may correspond to the developing structure accommodating the differential motion between the NW and SE Qaidam – South Qilian Shan blocks. It merges with the paleo-slab anomaly between Lake Hala and lake Qinghai and may reach the western termination of the Haiyuan Fault. See text for discussion.

Figure 1

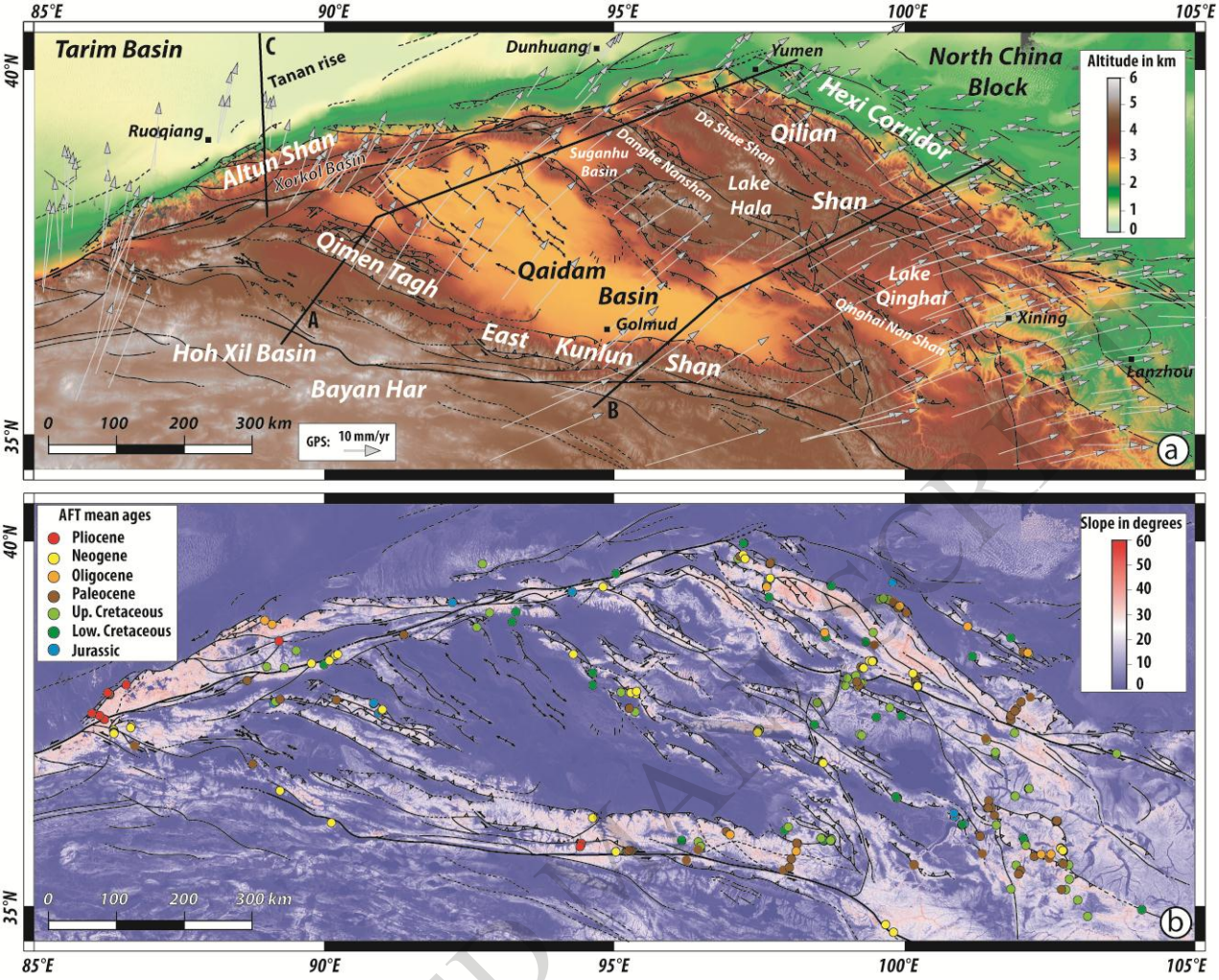

Figure 2

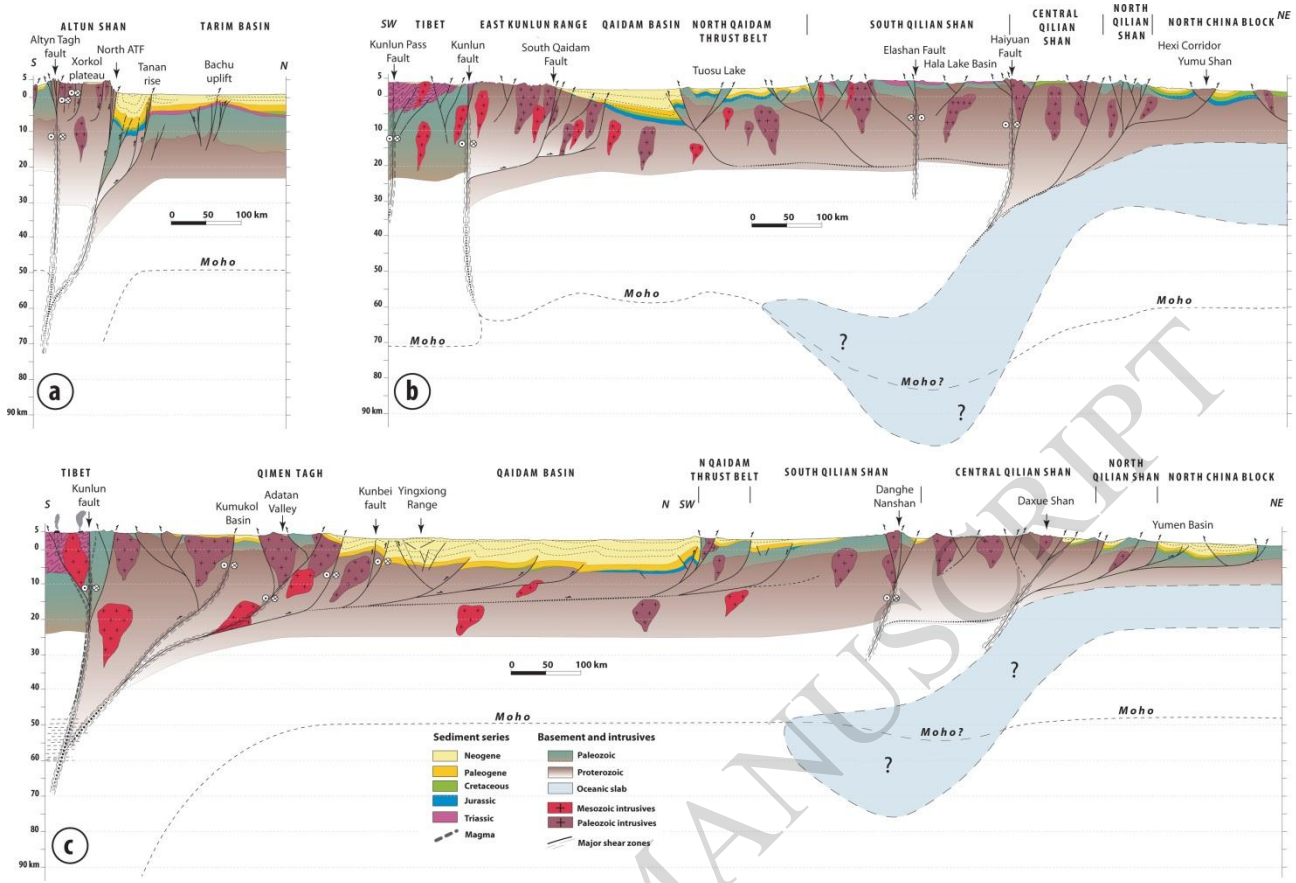

Figure 3

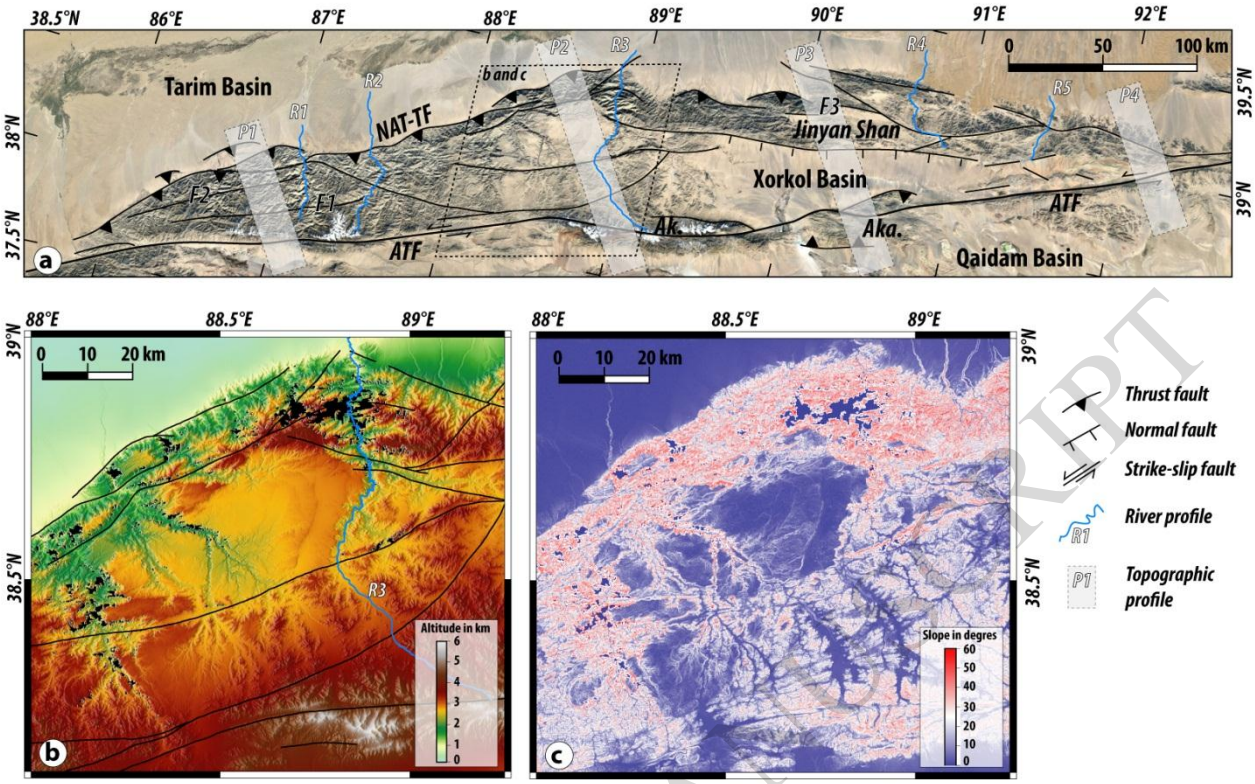

Figure 4

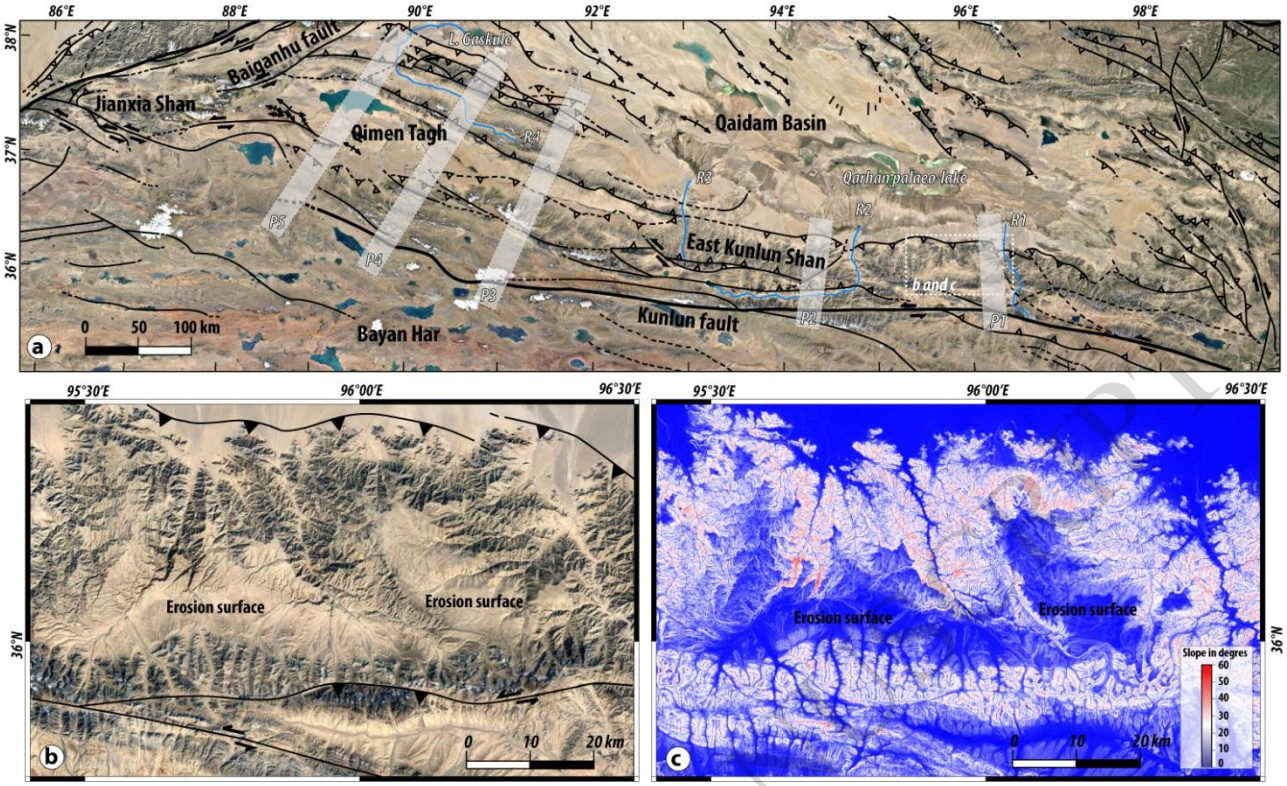

Figure 5

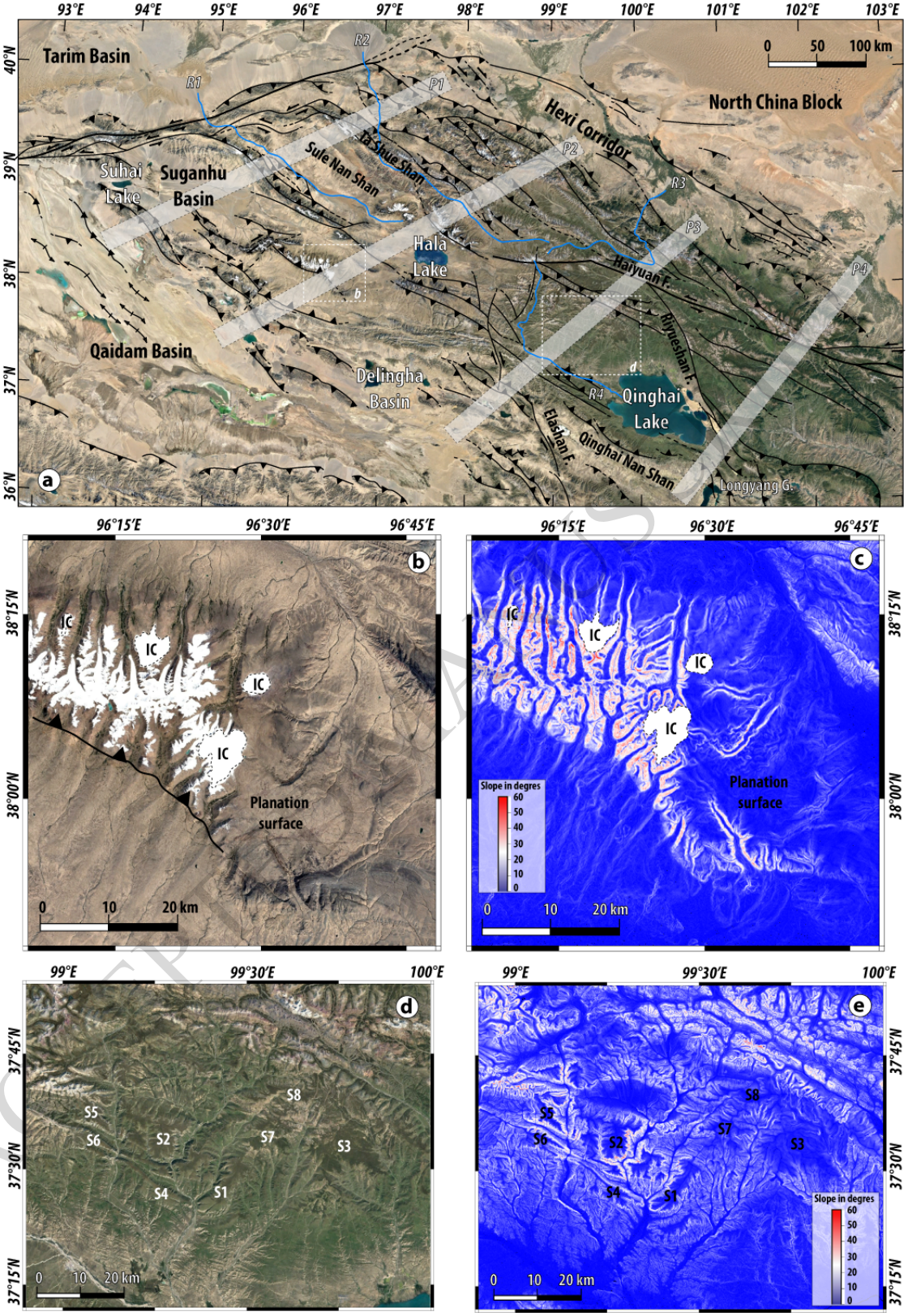

Figure 6

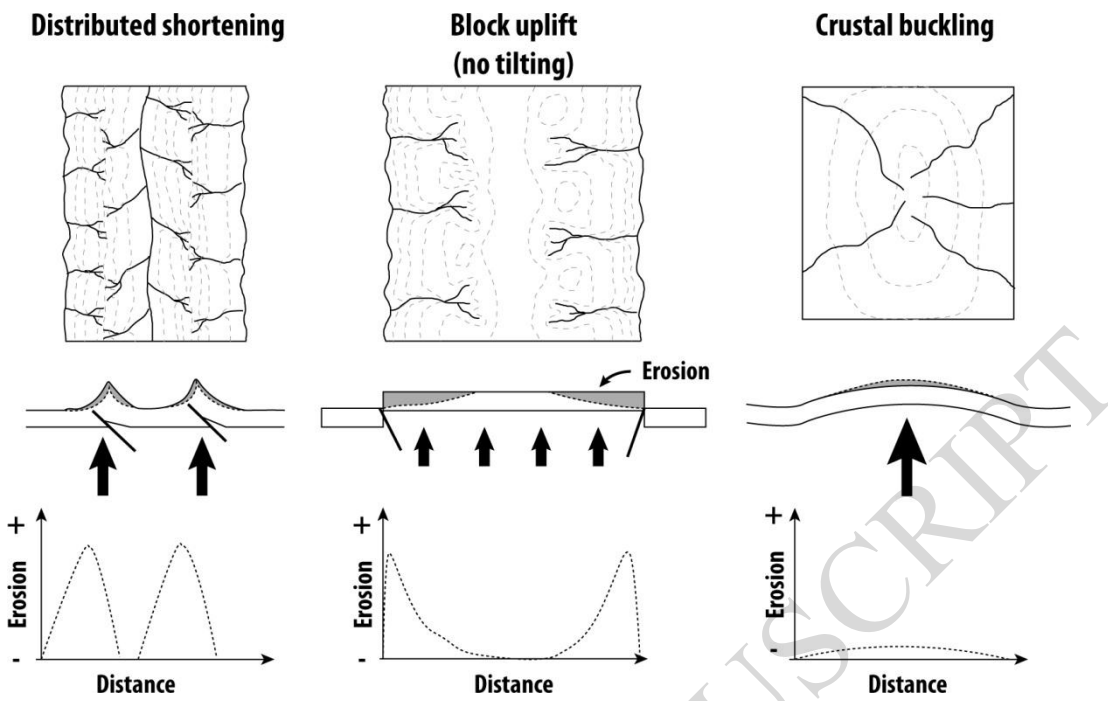

Figure 7

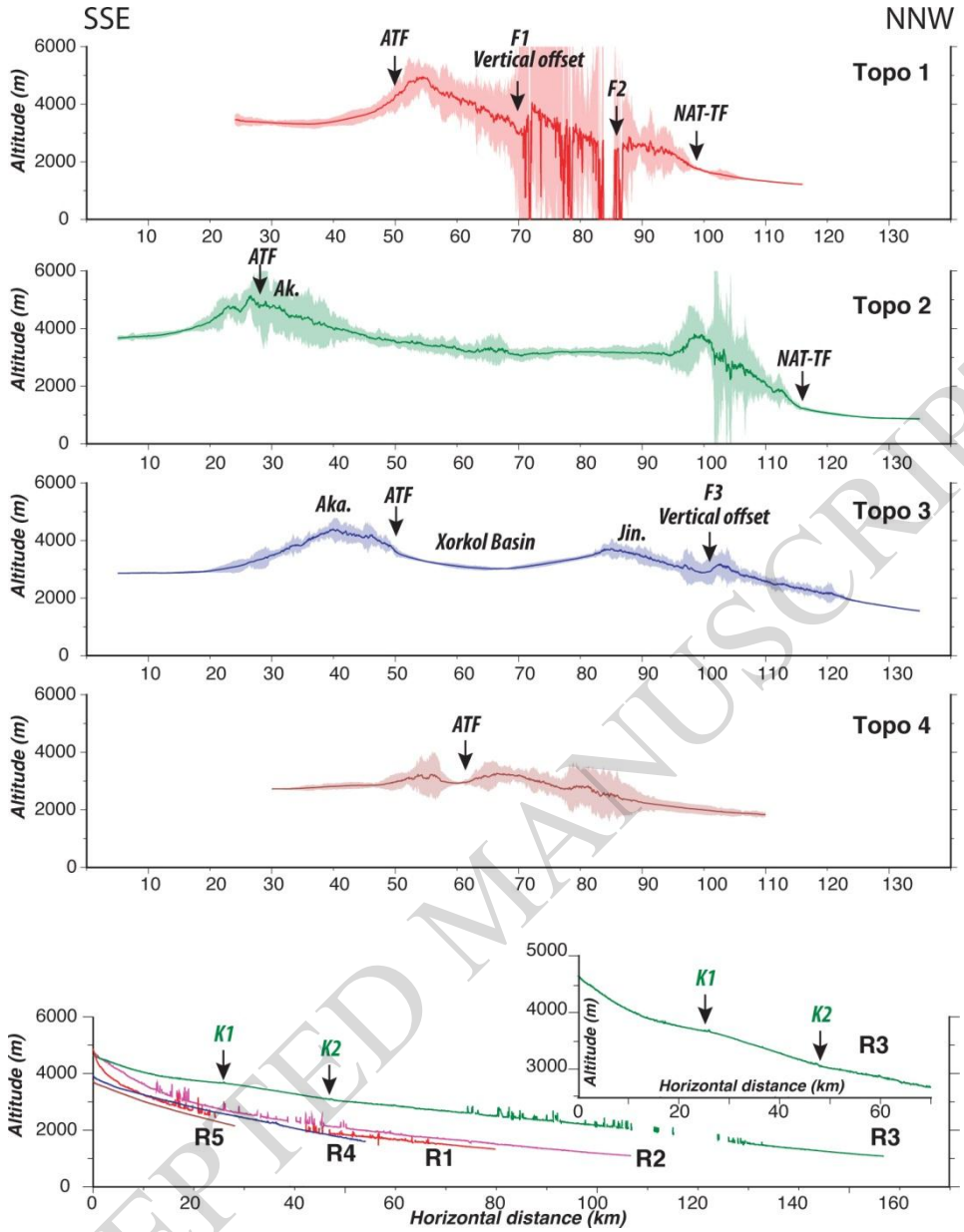

Figure 8

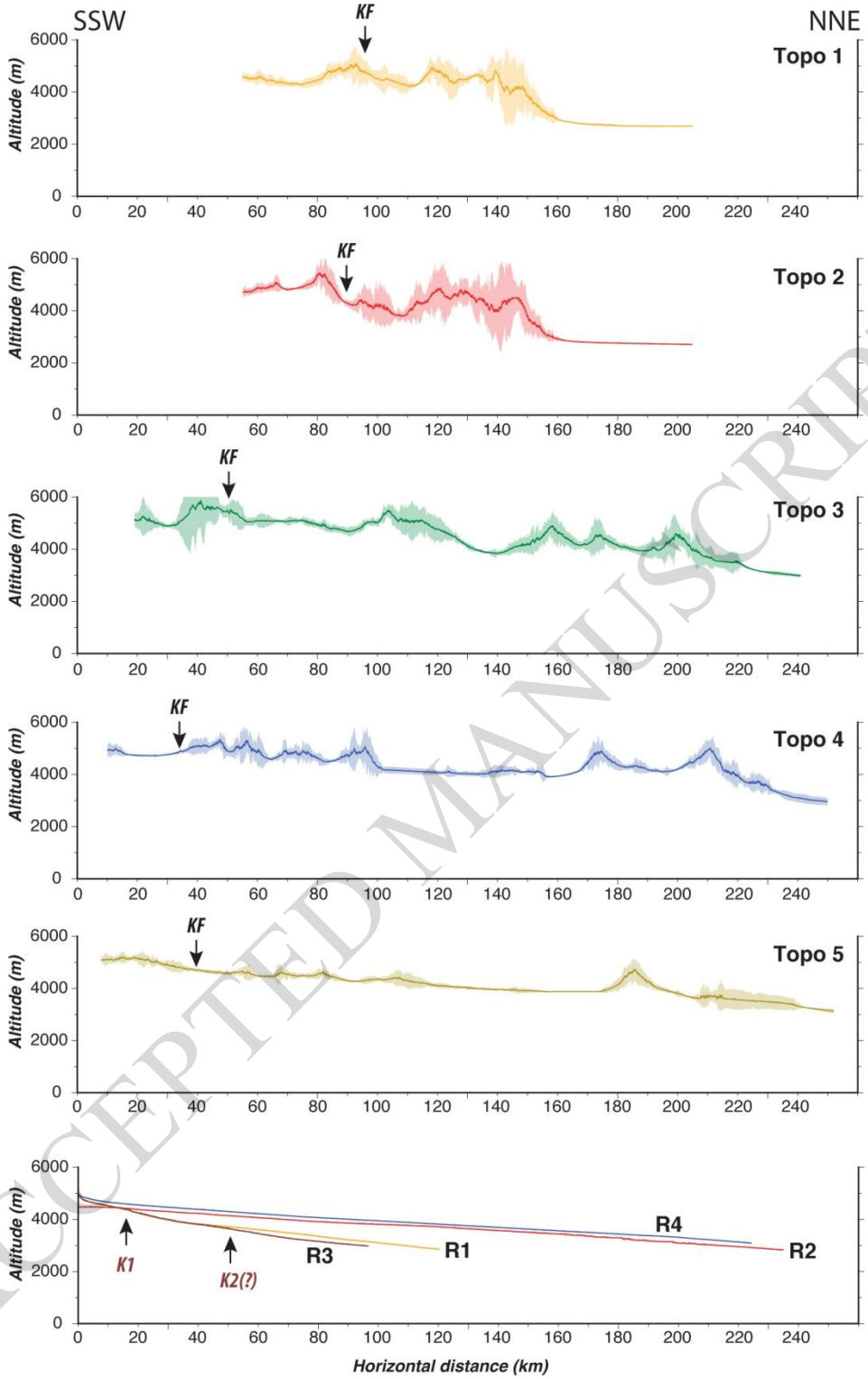

Figure 9

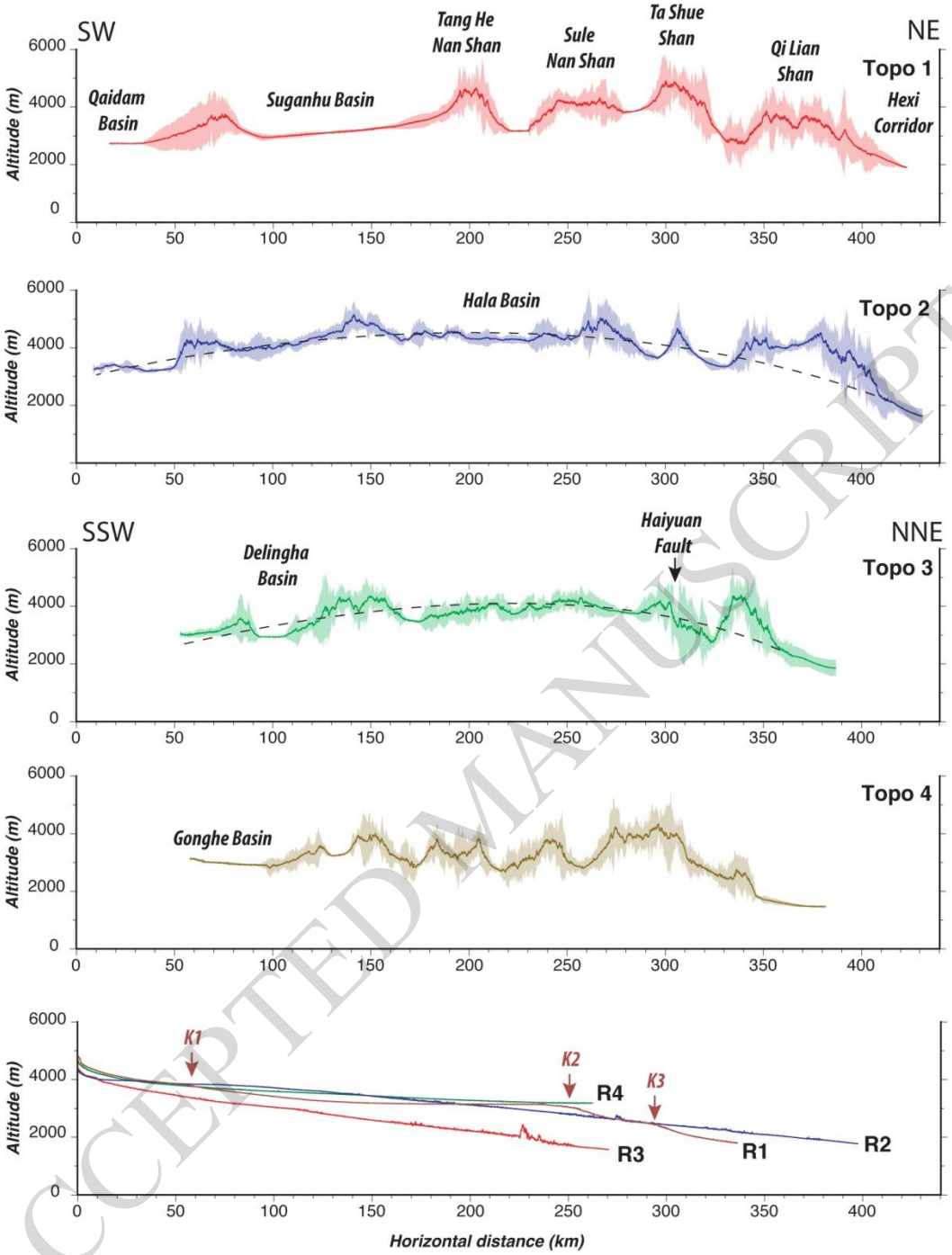

Figure 10

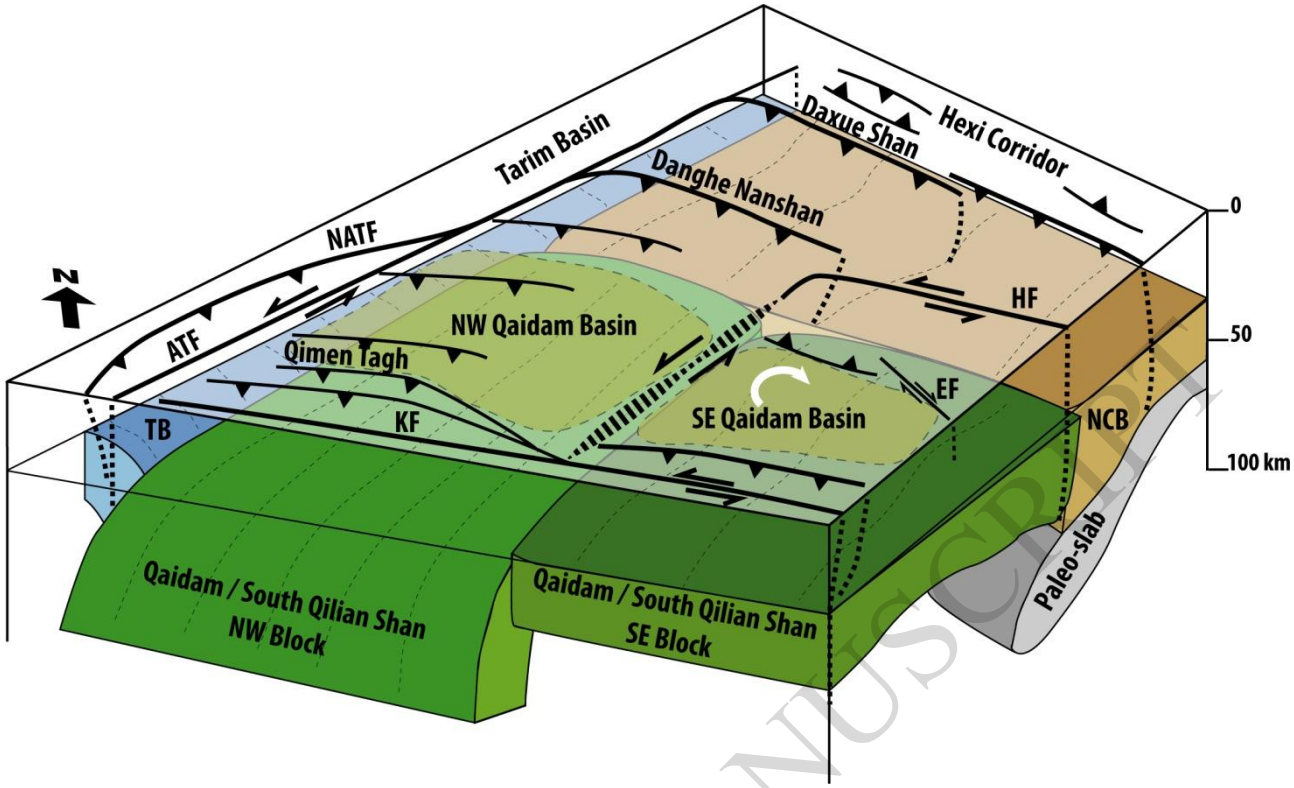

Figure 11